DNA 5268F

NUCLEAR BLAST RESPONSE OF AIRBREATHING PROPULSION SYSTEMS

Laboratory Measurements with an Operational J-85-5 Turbojet Engine

Michael G. Dunn

Calspan Advanced Technology Center
P.O. Box 400
Buffalo, New York 14225

31 March 1980

Final Report for Period 1 February 1979—31 March 1980

CONTRACT No. DNA 001-79-C-0155

APPROVED FOR PUBLIC RELEASE;
DISTRIBUTION UNLIMITED.

THIS WORK SPONSORED BY THE DEFENSE NUCLEAR AGENCY
UNDER RDT&E RMSS CODE B342079464 N99QAXAJ50405 H2590D.

Prepared for
Director
DEFENSE NUCLEAR AGENCY
Washington, D. C. 20305

Destroy this report when it is no longer needed. Do not return to sender.

PLEASE NOTIFY THE DEFENSE NUCLEAR AGENCY, ATTN: STTI, WASHINGTON, D.C. 20305, IF YOUR ADDRESS IS INCORRECT, IF YOU WISH TO BE DELETED FROM THE DISTRIBUTION LIST, OR IF THE ADDRESSEE IS NO LONGER EMPLOYED BY YOUR ORGANIZATION.

62704H

UNCLASSIFIED

SECURITY CLASSIFICATION OF THIS PAGE (When Data Entered)

REPORT DOCUMENTATION PAGE	READ INSTRUCTIONS BEFORE COMPLETING FORM
1. REPORT NUMBER: DNA 5268F	2. GOVT ACCESSION NO.: AD-A092
3. RECIPIENT'S CATALOG NUMBER: 2299	
4. TITLE (and Subtitle): NUCLEAR BLAST RESPONSE OF AIRBREATHING PROPULSION SYSTEMS. Laboratory Measurements with an Operational J-85-5 Turbojet Engine	5. TYPE OF REPORT & PERIOD COVERED: Final Report for Period 1 Feb 79—31 Mar 80
	6. PERFORMING ORG. REPORT NUMBER: Calspan Report No. 6486-A-1
7. AUTHOR(s): Michael G. Dunn	8. CONTRACT OR GRANT NUMBER(s): DNA001-79-C-0155 NEW
9. PERFORMING ORGANIZATION NAME AND ADDRESS: Calspan Advanced Technology Center, P. O. Box 400, Buffalo, New York 14225	10. PROGRAM ELEMENT, PROJECT, TASK AREA & WORK UNIT NUMBERS: Subtask N99QAXAJ504-05
11. CONTROLLING OFFICE NAME AND ADDRESS: Director, Defense Nuclear Agency, Washington, D.C. 20305	12. REPORT DATE: 31 March 1980 (17) J504 13. NUMBER OF PAGES: 66
14. MONITORING AGENCY NAME & ADDRESS (if different from Controlling Office) (12) 67	15. SECURITY CLASS. (of this report): UNCLASSIFIED 15a. DECLASSIFICATION/DOWNGRADING SCHEDULE: N/A

16. DISTRIBUTION STATEMENT (of this Report)

Approved for public release; distribution unlimited.

17. DISTRIBUTION STATEMENT (of the abstract entered in Block 20, if different from Report)

18. SUPPLEMENTARY NOTES

This work sponsored by the Defense Nuclear Agency under RDT&E RMSS Code B342079464 N99QAXAJ50405 H2590D.

19. KEY WORDS (Continue on reverse side if necessary and identify by block number)

Nuclear Blast Response
Airbreathing Propulsion System
Turbojet Engine

20. ABSTRACT (Continue on reverse side if necessary and identify by block number)

The work discussed in this report represents a technology development program in which an experimental technique has been developed for the performance of controlled laboratory measurements of simulated nuclear blast response of airbreathing propulsion systems. The technology program utilized an available J-85-5 turbojet engine located in the test section of the Calspan Ludwieg-tube facility. Significant modifications, described herein, were made to this facility in order to adapt it to the desired configuration. The J-85-5

DD FORM 1 JAN 73 1473 EDITION OF 1 NOV 65 IS OBSOLETE

UNCLASSIFIED

SECURITY CLASSIFICATION OF THIS PAGE (When Data Entered)

20. ABSTRACT (Continued)

engine had previously been used at Calspan for other purposes and thus came equipped with a total of eight pressure transducers at four axial locations along the compressor section. These transducers have a frequency response on the order of 40 KHz. Preliminary comparisons have been made between the measured pressure histories at selected compressor locations and predicted pressure histories using a simple computer code. The development of the code was initiated under this contract and completed as part of an ongoing IR&D effort at Calspan in computational fluid dynamics and problem areas related to engine dynamics.

TABLE OF CONTENTS

LIST OF ILLUSTRATIONS

Section 1
INTRODUCTION

Propulsion-system blast tolerance, including the relative importance of inlet flow distortion and internal blast-wave propagation, is governed by many factors. The engine type is of obvious importance; for example, turbojets, turbofans or ramjets, will respond differently to any given blast environment. For any particular engine type, the detailed internal gas-dynamic response will depend generally on the internal engine configuration, (the number and type of compressor and turbine stages, or combustor type), the engine operating point (stage pressure and stall-margin ratios, nozzle pressure ratio, turbine inlet temperature, and fuel/air ratio) and the engine control system (measurement parameters or response characteristics). The inlet type (internal, external, or mixed compression; high or low length-to-diameter ratio; and boundary-layer bleed and bypass provisions) can modify blast waves entering the engine from the front by changing the blast strength and introducing distortion. Finally, the local blast strength and orientation with respect to the propulsion system will strongly affect the transient internal engine pressures and temperatures that result.

A nuclear blast wave has associated with it a nearly step-function pressure and temperature pulse to which an operating engine may be subjected. The response of the propulsion system is recognized as an important consideration that must be treated in system studies utilizing airbreathing propulsion. Because this is a relatively new aspect of nuclear response, it is one for which only limited experimental and theoretical work has been done.

The only other similar laboratory measurement program that we are aware of is the one reported[1-3] by the Canadian group* at the Defence Research Establishment, Suffield. The purpose of the Canadian experiments was to test the general response of the Orenda 8 engine in contrast to the purpose of this program which was to develop a technology that could provide the detailed data necessary to predict the general behavior of airbreathing propulsion systems.

*In the early stages of the Calspan program (July 1978) representatives of Calspan, Kaman Avidyne, and R and D Associates visited the DRES people to discuss the two experiments.

Predictive codes that can be used to ascertain the transient engine behavior as a result of a pressure pulse do not appear to be available in the open literature. A few codes are available within certain organizations, but these are generally considered to be company proprietary and are not available. For this reason, a simple one-dimensional code based on existing technology was developed at Calspan in order to obtain an easy to use predictive capability. Several propulsion-system related computational schemes much more complex than the Calspan one-dimensional code are currently in various stages of development, but all are in need of verification data.

A technology program is described in this report whereby a significant portion of the data required to confirm the general validity of available predictive methods as they apply to turbojet engines has been obtained under controlled laboratory conditions. At the present time, the major portion of the United States airbreathing propulsion system inventory is composed of turbofans and not turbojets. However, the technology and the hardware developed during this program is directly applicable to a turbofan study, requiring basically only a change in engine.

In the remainder of this report, the facility modifications will be discussed in Section 2, a discussion of experimental results will be presented in Section 3, and a brief comparison between the compressor data and the one-dimensional code predictions will be presented in Section 4.

Section 2
EXPERIMENTAL FACILITY AND MODIFICATIONS

The basic Ludwieg-tube facility (sketched in Fig. 1), around which this technology program has been developed, was previously in existence at Calspan. The existing facility consisted of a supply tube (the driver gas supply) of 1.10-meters (42-inch) diameter by 18.3-meters (60-ft) long and the test section (in which the J-85 engine was located) which is 2.44-meters (8-ft) diameter by 18.3-meters (60-ft) long. The driver pressure limitation on the supply tube is 1379 Kpa (200 psia) which, as will be shown later, is almost a factor of ten greater than necessary to achieve the maximum allowable over-pressure for the J-85 engine. The experiments reported here required supply-tube pressures less than 25 psig. In order to convert the existing facility to one that could be used to develop blast vulnerability, several modifications were necessary.

An important restriction on the generation of shock waves to be directed into the engine is that the flow environment be free of foreign particles. It was thus necessary to modify the facility as shown in Fig. 2 so as to incorporate a driver technique[1-3] consisting of an actuating chamber and a flexible diaphragm in order to create a shock-wave environment free of diaphragm particles. A photograph of the actuating chamber and the flexible diaphragm (neoprene) is shown in Fig. 3. This chamber is initially pressurized to a static pressure approximately 2 to 5 psi in excess of the Ludwieg-tube driver supply tube in order to seal the flexible diaphragm against the shock-tube flange and support grid. The sketch shown in Fig. 2 illustrates that two additional tubes, in addition to the actuating chamber, had to be added to the facility in order to perform the desired experiments. The shock wave is initiated in the small diameter tube by rapid removal of the flexible diaphragm from the tube entrance. This is accomplished by venting the actuating chamber to the outside away from the engine by rupturing a mylar diaphragm by means of an air-operated knife. A shock wave is then formed in the 0.25-meter (10-inch) diameter tube (d) and progresses on to the larger diameter tube (D) where it weakens and eventually is directed into the operating engine. For steady-state operation of the engine

prior to initiation of a shock wave, the engine draws its supply air through the annulus bounded by the two tubes of diameters d and D as shown in Fig. 4. For the majority of the experiments to be described in this report, the engine was operated with an ASME bellmouth into which the shock wave is directed as illustrated in Fig. 4. The bellmouth is not rigidly coupled to the shock tube but rather a rubber transition piece attached to the shock tube fills the gap of approximately 3/4-inch between the tube and bellmouth. In this way, any impulse loading on the shock tube that may be created when the shock wave is initiated is isolated from the engine. Near the end of this report, a series of experiments is described for which the bellmouth is replaced by a 2-1/2° half-angle inlet and a transition section (engine hardware).

The experimental configuration sketched in Fig. 4 raises the question of possible reduced pressure at the bellmouth inlet and/or distortion as a result of the inlet air flowing through the long pipe (of diameter D) upstream of the inlet. The engine used in these experiments has previously been used at Calspan in the development of a rotating-stall control system. Therefore, there exists a large body of performance data obtained with the engine operating under ideal conditions. The engine performance while installed in the Ludwieg-tube configuration was checked against some of these previous results which are presented in Ref. 4. The results presented in this report were all obtained at corrected engine speeds in the range of 70% to 95%. The measured static pressure increase across the compressor and the stall-control system sensitivities indicated that the Ludwieg tube installation had associated with it a slightly lower inlet pressure and a relatively small amount of inlet distortion when compared to the previous measurements obtained for undistorted inlet flow. For the purposes of the blast-wave experiments of interest to this program, neither of these influences will compromise the results.

Figures 5 and 6 are photographs taken inside the receiver tank of the large diameter shock tube and the engine. Figure 6 illustrates the manner in which the shock wave is directed into the engine and the rubber fairing which isolates the shock tube from the engine. This photograph demonstrates that a portion of the bellmouth is not in use which could account for some of the steady-state distortion discussed above. Several of the static pressure taps

in the large diameter pipe can also be seen on the photograph given in Fig. 6. A description of transducer locations in both the small and large diameter shock-tubes is given in the next section.

2.1 SHOCK-TUBE AND ENGINE INSTRUMENTATION

Figure 7 is a sketch of the instrumentation locations in the shock tubes. In addition, the overlap of the large diameter tube relative to the smaller tube and the distance from the tube exit plane to the compressor force are also illustrated. The ratio of shock-tube diameter to entrance tube diameter, d/D, and the overlap length were sized on the basis of calculations[5] performed by Kaman AviDyne. Later in this report, measurements obtained at each of these instrumentation locations will be presented in detail and the call-outs are consistent with those given on Fig. 7. The transducers located at P_1 to P_5 are Kistler, Model 603A gages and those located at P_6 to P_9 are Calspan constructed gages.

Total-pressure time histories were obtained at two locations in the large-diameter tube just upstream of the compressor face. These transducers were not installed while the transient engine-response data were being obtained, but were rather used to obtain detailed shock-tube performance data at times when engine data were not being taken. Two Calspan constructed transducers were used to perform these measurements and the results will be described in Section 3. The pressure transducers used here were calibrated before and after the experiments and the calibrations appear on the data records presented in Section 3.

It was mentioned earlier that a 2.5° half-angle inlet was constructed and instrumented so that the change in transient engine response with an inlet could be compared to the response obtained with the bellmouth. This particular inlet was not intended to represent the flight hardware inlet, but rather the purpose was to use a known inlet geometry and obtain transient pressure histories at various locations so as to provide verification data for the Kaman AviDyne BID code. The transition section used with flight hardware in coupling the flight inlet to the engine was also used in this setup. A photograph of the inlet used here is presented in Fig. 8 and a sketch of the experimental configurations is given in Fig. 9. The pressure transducers placed at 10 locations along the inlet

were Piezotronics pcb-pzt-37-21 types. A 50% open plate was placed at the exit plane of the outer cone in an attempt to cancel the rarefaction fan, originating at that location, with a reflectd shock wave. No attempt was made to refine the porosity of the plate so as to tailor the reflection. The pressure histories measured in the inlet with the engine at rest indicated that the porous plate technique resulted in a reasonably uniform inlet flow for a period of time on the order of 40 milliseconds.

The engine used for the measurement program described here has been used at Calspan for several years to study stall control systems. The Defense Nuclear Agency borrowed the engine and associated instrumentation from the Air Force Aeropropulsion Laboratory. No additional instrumentation was installed on the engine beyond what was already there for the stall control studies because these initial experiments were considered to represent a demonstration-of-technology effort. Therefore, the engine instrumentation locations described here were placed for the purpose of studying rotating stall and not specifically for blast-effects studies.

The front portion of the compressor of the GE J-85-5 engine used for these experiments is instrumented[6] with eight Piezotronic pressure transducers (20 to 40 KHz response) as the photograph presented in Fig. 10 illustrates. The eight transducers are located at four axial locations with two at each of the following locations:

(a) near the first stage rotor mid-chord; (1RMCT, 1RMCL)

(b) near the quarter-chord of the first stage stator, as close to the stator suction surface as possible; (1SQCT, 1SQCL)

(c) between the second stage stator trailing edge and the third stage rotor leading edge; (2STET, 2STEL).

Two additional pressure transducers are located near the rear of the compressor as illustrated in the photograph of Fig. 11 between the seventh stage stator blades at approximately mid-chord (7SMCL). However, because of engine geometry, these transducers could not be flush-diaphragm mounted and thus the frequency response is less than that of the forward transducers.

In addition to the pressure measurements noted above, one other pressure transducer is installed on the engine. This transducer is used in conjunction with those noted above to measure the static pressure rise across the compressor, and is located at the throat of the bellmouth upstream of the compressor face.

An accelerometer is mounted on the compressor casing from which the peak-to-peak displacement history can be deduced using a suitable electronics package. Time histories of compressor casing displacement were recorded along with the engine pressure histories and are discussed in Section 3.

Section 3
DISCUSSION OF EXPERIMENTAL RESULTS

This section of the report has been divided into three separate discussions: (1) basic shock-tube and engine data with the compressor at rest, (2) shock-tube and engine measurements obtained with the bellmouth attached to the engine as sketched in Fig. 4, and (3) measurements obtained with the 2.5° half-angle inlet attached to the engine as sketched in Fig. 9. The J-85 is equipped with bleed doors located just aft of the first stage of the compressor. These bleed doors are normally open or partially open until the corrected engine speed has exceeded approximately 93%. It was previously noted that the engine used in this work was equipped with a Calspan-developed stall control system. However, this stall control system was not intended for use when the corrected engine speed was as large as 93%. Blast-wave experiments were performed for specific engine conditions both with the stall control system active and with it inactive. The data records will clearly note whether or not the control was active. If the control was off then the bleed door position was under control of the normal engine schedule. The reason for activating the stall control system during some of the early blast-wave experiments is that it was felt that if the engine were to be forced into rotating stall or surge as a result of the blast-wave environment, then recovery might be enhanced by opening the doors and relieving the pressure on the front portion of the compressor. The results that are presented in this section illustrate that the compressor behaves differently with the stall control active compared to when it is inactive, but in neither case can evidence of rotating stall or surge be found.

3.1 BASIC SHOCK-TUBE DATA AND ENGINE DATA WITH COMPRESSOR AT REST

A sketch of the locations of all of the shock-tube instrumentation is given in Fig. 7, a sketch of the inlet instrumentation is given in Fig. 9, and photographs of the engine instrumentation are given in Figs. 10 and 11.

Figures 12(a) and 12(b) are representative of the shock-tube data obtained. Pressure transducers P_1-P_5 are in the sidewall of the 10-in diameter tube, transducers P_6-P_9 are in the sidewall of the 22-in diameter tube, and the

total pressure probes were located on the centerline and 2-inches off of the centerline of the 22-in diameter tube. Pressure transducer P_5 is located at approximately six inches from the open end of the 10-in diameter tube. The upstream moving expansion fan as a result of the shock wave exiting from the open end of the shock tube can be observed at this location and it can be traced back upstream to location P_1. The characteristic of the pressure pulse at location P_5 makes it attractive for time sequencing the three CEC recorders.

Throughout this report we refer to a value "Δp at the compressor face". This value is obtained from the P_9 data record as illustrated on Fig. 12(a). The peak pressure occurring at early time on the P_9 data record is a result of the reflection of the incident shock wave from the compressor face. This reflected wave can also be traced back up the 22-in diameter tube and into the 10-in diameter tube.

The duration of the useful shock-tube test time is noted on Fig. 12(a). This time represents the duration of uniform conditions at the compressor face as a result of compressing the gas initially contained in the 10-in and 22-in diameter tubes. Pressure peaks and valleys occurring after the test time are associated with the driver gas and are thus not relevant to the experiment being performed.

In order to relate the pressure increase measured at P_9 (Δp) to an equivalent blast-wave overpressure, one must account for the increase in incident shock pressure as a result of the reflection from the compressor face. Figure 13 has been obtained from the data by reading the first plateau pressure occurring in the P_6, P_7 and P_8 pressure records and comparing that reading to the Δp marked on the P_9 trace. As can be seen from Fig. 13, a 2.0 psi blast-wave overpressure results in a pressure increase at the compressor face corresponding to approximately 2.5 psi.

Figure 12(b) includes a comparison between the compressor casing displacement history and two total-pressure histories taken in the 22-in diameter tube. The characteristics of the total pressure records and the corresponding pressure levels are in good agreement with the P_9 data presented in Fig. 12(a).

Note that the maximum total pressure is associated with that period of time called shock-tube test time. It is illustrated in Fig. 12(b), and will be shown several times later in this report, that the peak in the compressor vibration occurs much later in time than the peak total pressure. The contribution of the late time flow (after the test period) to the vibration response can not be conclusively determined at this time. Table 1 is a summary of conditions for which casing vibration data are available. This table demonstrates that the magnitude of the casing displacement increases rapidly with overpressure but it is a relatively weak function of engine speed. Data are presented both with the engine operating and with the engine at rest to demonstrate this point. The largest displacement value was obtained at 93% corrected engine speed with the stall control-system active. The data did suggest that slightly increased compressor displacement occurred with the stall control-system active.

Since the purpose of this experimental program was to investigate the transient response of the engine to a shock wave incident on the compressor face, it was necessary to obtain a baseline measurement with the bleed doors closed and the engine at rest. Recall that this engine is equipped with bleed doors and that at corrected speeds in excess of approximately 93% these doors are closed. Most of the data will be taken at these higher corrected speeds and the stall control system will be inactive so that the bleed doors will remain closed, thus the reason for obtaining the baseline data with doors closed.

Figures 14(a) and (b) are the shock-tube pressure histories, the engine pressure histories and the compressor-displacement time history obtained for a Δp of 3.9 psi at the configuration conditions discussed above. For these experiments, the total pressure probes have been removed from the 22-in diameter tube. The characteristics of the shock-tube data records presented in Fig. 14(a) are very similar to those presented in Fig. 12(a) and (b). The engine pressure histories illustrate that the incident shock moves through the machine at a propagation velocity approximately equal to its velocity in the 22-in diameter tube. The early time peak-pressure pulse is followed by an uniform pressure pulse the shape of which is consistent with the P_9 pressure record. These characteristics of the engine pressure records change significantly when the engine

is operating as will be demonstrated later. Figure 14(b) illustrates two of these engine pressure histories, 2STET and 2STEL, the compressor casing displacement history, and the P_5 record. From Fig. 14(b) it can be seen that the peak compressor-casing displacement occurs at approximately 230 ms after shock arrival at the compressor face. This displacement and time history is essentially the same as that measured when the machine was operating at high corrected speed as will be shown in the next sub-section.

3.2 SHOCK-TUBE AND ENGINE MEASUREMENTS OBTAINED WITH BELLMOUTH ON ENGINE

With the ASME bellmouth attached to the engine and the experimental configuration shown in Figs. 6 and 7, a series of experiments were performed to investigate the performance of the J-85-5 turbojet engine under simulated nuclear-blast environments. Measurements were performed with the engine operating at corrected speeds in the range of approximately 93 to 95% for equivalent blast-wave overpressures in the range of 0.8 psi to 2.5 psi.

In addition to the shock-tube and engine pressure histories described above, two brush recorders were used to record time histories of engine rpm, bleed-door position, static-pressure increase across the compressor, and pitot pressure in the bellmouth from which weight flow rate can be calculated. The second of these brush recorders was used to record four engine pressure-transducer histories on a much slower sweep rate than that used on the CEC recorders.

Figures 15(a) and (b) present typical data for an engine operating point of 93% corrected speed, with a Δp= 1.0 psi and the stall control off. From Fig. 15(a), it can be observed that the engine speed remains essentially constant for the 1.0 psi overpressure condition. The bleed doors remain closed during the entire time but the reference pressure (Δp_{ref}) indicates a sharp increase indicating the shock passage through the compressor. The particular transducer giving this record is a differential transducer with the low side connected to a static pressure port just upstream of the compressor face in the straight portion of the bellmouth and with the high side connected to a static port just downstream of the last compressor stage. The specifications

on this instrument indicate that the diaphragm frequency response is on the order of 500 to 700 Hz with the high-pressure side responding faster than the low side. The reason for the increase in (Δp_{ref}) when the shock wave passes through the machine is that the overpressure pulse is magnified by the compression ratio of the machine (as will be illustrated later during discussions of Fig. 16(c)) so that the downstream side of the transducer sees a large pressure pulse associated with the initial passage of the shock-wave through the machine. After passage of this initial wave system, the differential transducer is essentially reading a pressure differential approximated by the difference between the 7SMCL and 1SQCL engine transducers to be discussed later. However, it is almost impossible to make a time history comparison because the engine transducers have a frequency response on the order of 20 to 40 KHz but the differential transducer is responding at approximately 500 to 700 Hz. By using the pitot pressure history shown at the bottom of Fig. 15(a), the weight flow can be calculated. The transient response of this pitot pressure record is not sufficient to obtain meaningful data for the time interval associated with the presence of the overpressure at the compressor face. It should be noted that the weight flow does not go to zero as indicated by the recorded signal.

The second brush recorder was used to record four engine pressure histories on a slower sweep rate than was used on the CEC recorder. The same engine pressures are presented, along with the shock-tube data on Fig. 15(c) for a sweep speed four times faster than that used on Fig. 15(b). Engine pressures 1RMCT (first stage rotor mid-chord top), 1SQCT (first stage quarter-chord top), 2STET (second stage stator trailing-edge top) and 7SMCL (seventh stage stator mid-chord left) were selected for the larger sweep rate display. These pressure histories are consistent with those presented in Fig. 15(c) and indicate that events occur essentially simultaneously, compared with one engine revolution ($\sim$ 4 milliseconds). It can be seen from the records presented in Fig. 15(b) that the peak engine pressure is associated with the passage of the initial wave system through the machine. It can also be noted that the compressor regains its initial operating pressure level at approximately 1200 milliseconds after arrival of the shock but it should be recalled from the total pressure histories presented in Fig. 12(b) that this post test-time disturbance is the result of the driver gas and not the shock processed gas.

Figure 15(c) presents the shock-tube and engine pressure histories on a sweep rate of four times the sweep rate used on Fig. 15(b). The four engine pressures presented on Fig. 15(b) are also included on Fig. 15(c). The general shape of these engine pressure histories should be compared with those shown in Figs. 14(a) and (b) for the engine at rest. The first 10 ms or so of these data records are similar but then the engine pressures shown on Fig. 15(c) return to their pre-shock values suggesting that possibly the turbine stage was operating very nearly choked and could not accommodate the increased weight flow associated with the shock-processed gas. As the shock overpressure is increased at the higher corrected speeds, this general character of the engine pressure records will become more pronounced. Figure 15(d) isolates two engine pressure records, 2STET and 2STEL so that their histories can be observed more closely. These particular transducers were selected because they are located at a station in the compressor corresponding to one of the lumped volume sites consistent with the machine code to be discussed later. The bottom trace on Fig. 15(d) is the compressor casing displacement history. It can be seen from this record that the peak displacement occurs at approximately the same time after shock reflection as it did for the compressor at rest.

Figures 16(a) to (d) are similar to those just presented but for an overpressure at the compressor face of 2.2 psi. The engine speed record shown on Fig. (a) indicates a small ($\sim 0.6\%$) speed increase as a result of the shock-wave passage. The other traces shown on this data record are similar to those shown previously. It should be recalled that the indicated sudden drop in mass flow is an instrumentation transient response problem and is not felt to be a physical engine event.

The results presented in Figs. 16(a), (c) and (d) can be used to demonstrate that the overpressure imposed at the compressor face is magnified in passing through the compressor by the compression ratio. From Fig. 16(a), it can be determined that the steady-state operating Δp_{ref} was on the order of 60.5 psi, the corrected speed was about 93.7%, and q_c = 36 in H_2O, which translates into a weight flow of about 41.8 lb/sec. Using this weight flow, the corrected speed, and the operating map for the machine, one can calculate the static pressure rise across the first seven stages (for

comparison with 7SMCL) to be approximately 3.89. For this particular experiment, the measured pressure at station P_9 was 2.2 psi and the peak pressure measured at 7SMCL was 8.63 psi giving a compression ratio of 3.92 which is in good agreement with the estimated compression ratio. This same calculation was performed for the data presented in Fig. 17 for a corrected speed of 94.3%. For this case, the Δp_{ref} was 61.8 psi, the weight flow was 42.4 lb/sec and the estimated static pressure rise across seven stages was 4.3. The measured overpressure at the compressor face was 3.3 psi and the peak pressure at 7SMCL was 13.6 psi giving a measured compression of the overpressure equal to approximately 4.1. This same comparison was made for all of the data with the same general result.

The compressor casing displacement history and two selected engine pressure histories are shown in Fig. 16(d). The compressor casing displacement can be seen to reach a maximum at a time consistent with that shown on Fig. 14(b) and the increase in displacement with shock overpressure can be observed by comparison with Fig. 15(d).

The highest overpressure for which engine measurements were obtained with the stall control off was 3.3 psi and typical results for this experiment are given in Fig. 17. The selected engine pressure histories shown in Fig. 17(b) illustrate a characteristic similar to that obtained for Δp = 1.0 and 2.2 psi but with larger amplitudes as would be expected. Comparison of Figs. 15(b), 16(b) and 17(b) as well as the engine pressure histories presented in Figs. 15(c), 16(c) and 17(c) does not suggest any evidence of rotating stall or surge as we are accustomed to seeing it on a transient basis. In addition, the engine did not flame out or suffer any severe damage during the course of these experiments. The comparison cited above does indicate that with increasing overpressure, the compressor pressures return to their pre-shock level or flow at an earlier time. For the Δp = 3.3 psi case, the local pressures fall somewhat below their pre-shock values. One can trace the movement of the return to pre-shock operating point from the rear of the compressor (7SMCL) towards the front (2STEL, 1RMCL) suggesting that the turbine was probably operating near a choked condition and could not accommodate all of the increased weight flow associated with the shock wave. This observation would suggest that for modelling the

engine performance when subjected to a blast-wave environment, it is important to include detailed information about the entire machine. The increase of compressor casing displacement with increasing overpressure can be observed on Fig. 17(d). A displacement of 0.006 inches is near the recommended limit for the engine.

Several experiments were performed with the stall control system on over a range of corrected engine speeds and overpressures values. Typical shock-tube and engine pressure histories from one of these experiments is shown in Figs. 18(a) and (b). The results presented in Fig. 18 can be compared with those given in Fig. 17(a) and 17(c) since the corrected engine speed and the overpressure level are approximately equivalent. The rapid movement of the bleed doors when the overpressure associated with the shock wave is sensed as illustrated on the bottom trace of Fig. 18(a). The character of the $(\Delta p)_{ref}$ trace can also be seen to be considerably different in the two cases. Perhaps the most dramatic influence of the stall control system can be seen for the engine pressure histories of Fig. 18(b). The pressure histories for the initial 20 milliseconds after shock arrival are similar but beyond that time the general characteristic changes significantly. There also appears to be a 5 Hz oscillation in the engine pressure records that persists for approximately three or four cycles. Sufficient supporting data are not available at the present time to explain the behavior question any further because the engines of future interest are not equipped with stall control systems of this type.

3.3 MEASUREMENTS WITH 2.5° INLET

It was noted earlier that a 2.5° half-angle inlet (see Fig. 8) was constructed and located on the engine in place of the bellmouth as illustrated in Fig. 9. Several shock-tube experiments were performed over a range of overpressure values with the engine at rest in order to verify the performance of the 50% open porous plate at the exit plane of the inlet and in order to obtain baseline pressure distributions along the inlet. The results of these measurements indicated that the porous plate performed satisfactorily as evidenced by a uniform pressure level along the length of the inlet for a period of time on the order of 40 milliseconds.

Upon completion of the measurements discussed above, the engine was started and an attempt was made to obtain inlet and engine pressure data when the inlet was subjected to shock waves. Before starting the engine, the porous plate was covered with mylar so that the engine would not draw air from the rear of the cone and thus cause a separation bubble at the inlet leading edge. With the 2.5° half-angle inlet installed, the engine would not perform as it had previously with the ASME bellmouth. The engine pressure records shown in Fig. 19 suggested that at idle speed the engine was on the verge of rotating stall. Comparison of Fig. 19 with Figs. 15(b), 16(b) and 17(b) gives an indication of the engine performance. The engine speed was gradually increased to 71% where is went into rotating stall and the throttle was chopped. The engine pressure records of Fig. 19 indicate that this stall was accompanied by a large pressure fluxuation. Subsequent attempts to start the engine were unsuccessful, and upon inspection of the inlet the leading edge was found to be bent. At this time, the experiments were terminated and it was concluded that a redesigned inlet leading edge would be necessary in order for the engine to perform satisfactorily.

Section 4
COMPARISON OF ENGINE PRESSURE HISTORIES WITH MEASUREMENTS

Earlier in this report it was noted that a theoretical or empirical methodology is needed for determining and evaluating the blast response of air breathing propulsion systems. In the early stages of this program an attempt was made to develop a simple one-dimensional code using the "simplified volumetric method" of Jansen, et al.[7] supplemented by a relaxation-type equation in order to meet this need. Unfortunately, this version of the code encountered difficulties in that the pressure results appeared to oscillate after the initial reflection of the shock wave from the first-stage compressor row. A review of this problem was presented to DNA representatives and the DNA consultants in April 1979, and it was decided to discontinue this particular effort.

As part of an ongoing IR&D effort in computational fluid mechanics at Calspan, problem areas related to engine dynamics are being investigated. Therefore, the basic idea of this simple blast-wave code was implemented in this broad IR&D interest and has subsequently been developed to a point where relevant predictions[8] can be performed for engine experiments of interest here. This work is not yet completed, but it is to a point where the necessary modifications to the code are now understood. The results presented in this section are taken from Ref. 8 as is much of the description.

4.1 BRIEF REVIEW OF FORMULATION

Calculating the transient response of an air breathing propulsion system when it is subjected to a blast wave is essentially a problem of following the propagation, reflection, and interaction of a wave through a variable-area duct with localized energy addition. It would appear that the method of time-dependent characteristics would be well suited for the problem, as it is the most accurate and stable of the available techniques and, in addition, yields the clearest representation of the phenomena. However, the program logic required to keep track of the numerous waves and their reflections tends to become unmanageable. On the other hand, the easily programmed finite-difference

schemes tend to develop stability problems. Since both Refs. 7 and 9 found that the time increments necessary for following the unsteady phenomena were less than those imposed by stability requirements, and since Ref. 7 found good agreement between the finite-difference and method-of-characteristics results, the finite-difference technique was chosen.

The differential equations of the "simplified volumetric method" are derived in Refs. 7 and 9 by applying the laws of mass and momentum conservation to a control volume. For the i^{th} volume, one obtains

$$\frac{d\bar{W}_i}{dt} = \frac{\bar{A}_i g_o}{\bar{z}_i} \left(P_i \pi_i - P_{i+1} \right) \tag{1}$$

$$\frac{d\bar{P}_i}{dt} = \frac{\gamma R \bar{T}_i}{g_o \bar{A}_i \bar{z}_i} \left(W_i - W_{i+1} \right) \tag{2}$$

where the superior bar indicates a mean value over the i^{th} volume, P_i is the total pressure at station i, W_i is the weight flux (lbf/sec) at station i and π_i is the pressure ratio across whatever compressor stage happens to be in volume i. The mean total temperature $\bar{T}_i$ is supposed to be constant in time and to be evaluated in such a way that the relation

$$\frac{d\bar{P}}{dt} = \gamma R T \frac{d\rho}{dt} \tag{3}$$

is true. The pressure ratio π_i is set = 1 in blade-free spaces such as the inlet and tail pipes. In the compressor,

$$\frac{d\pi_i}{dt} = \frac{1}{\tau_i} \left(\pi_i^{ss} - \pi_i \right) \tag{4}$$

where π_i^{ss} is the quasi-steady pressure ratio obtained from the steady state characteristics map at the transient corrected weight flow,

$$\omega_i = \frac{W_i \sqrt{T_i / T_{ref}}}{P_i / P_{ref}} \tag{5}$$

The characteristic relaxation time τ_i' is assumed to be half of the blade passage time.

$$\tau_i = 0.5\, z_i / u_i' \tag{6}$$

It should be noted that Equations (4) and (6) are pure assumptions.

The differential equations (1), (2) and (4) must be solved subject to the boundary conditions

$$P_1 = P_1(t) \tag{7}$$

$$W_N = f(P_N, T_N, A_N, p_\infty) \tag{8}$$

where N is the last station (Fig. 1) and p_∞ is the ambient static pressure. Both Refs. 7 and 9 took care to shape the input pulse $P_1(t)$ so as to avoid interactions between the input pressure disturbances and the reflected pressure waves and neither reference considered positive pressures. Unfortunately, the luxury of carefully selecting the pulse shape is not permitted here since we regard $P_1(t)$ as an arbitrary, bounded and continuous function of time.

4.2 COMPARISON OF PREDICTION WITH MEASUREMENTS

The equations given above have been solved as described in Ref. 8 using available information from the engine manufacturer as input parameters. Figures 20, 21 and 22 are comparisons between the predicted pressure histories and the measured pressure histories at a location within the compressor between the second stage stator trailing edge and the third stage rotor leading edge. For each of these calculations, the experimentally determined pressure history at a location approximately 27 inches upstream of the compressor face in the 22-in diameter pipe was an input. In all cases for which calculations were performed, it was found that the code gave good predictions of the peak pressure, but the predicted pressure history did not fall off as rapidly as the measured pressure. The reason for this is felt to be due to the fact that, at the present time, the code only models the compressor and not the turbine. It is well known that when the machine is operating at 93 to 95% corrected speed, the turbine is nearly

choked. Under these conditions, the turbine would be the factor controlling the machine behavior and must be included in the model before good comparison between prediction and data will be obtained for the pressure history. This addition to the code represents a relatively minor addition.

Section 5
CONCLUSIONS

The material presented in this report describes the results of a technology development program at Calspan Corporation. The initial experimental phase of this program utilizing a GE J-85-5 turbojet engine has been completed. At the present time, it is possible to conclude the following:

- A facility has been developed at Calspan that can be used to obtain controlled laboratory data for the study of the influence of blast waves on air breathing propulsion systems.
- The turbojet engine used in this technology development program did not appear to stall or surge for overpressures up to $\Delta p)_{\substack{\text{Blast} \\ \text{Equivalent}}} = 2.5$ psi.
- The shock-wave overpressure imposed on the compressor front face is amplified as it passes through the machine by an amount approximately equal to the compression ratio of the compressor.
- A simple one-dimensional machine code developed at Calspan was used to demonstrate good agreement between predicted and measured peak pressures in the compressor. However, the time histories did not agree well, perhaps because the turbine was not included in the model.
- For turbojet engines encountering blast waves, it is important to consider induced vibrations in the compressor section.
- At high engine speed, the turbine gas dynamics appear to control the response of the compressor to the imposed pressure pulse.

Section 6
RECOMMENDATIONS

- The Calspan one-dimensional machine code should be modified to include the turbine stage. Upon completion of this modification, comparison could be made between the measured and predicted compressor pressure histories.
- The feasibility of the experimental technique has been demonstrated on a turbojet engine. It is appropriate that the turbojet be replaced with a turbofan engine (specifically instrumented for blast-wave testing) and an appropriate series of experiments performed.
- Blast-wave response of the turbofan engine should be investigated for the inlet at angle of attack or yaw.
- The feasibility of directing blast waves into the exhaust pipe of the turbofan engine should be investigated.
- The feasibility of using ejectors at the exhaust region so that sub-atmospheric (simulated higher altitudes) experiments could be performed should be investigated.

Section 7
REFERENCES

1 Muirhead, J.C., Naylor, R. and Felt, G.D., "The Transmission of Blast Waves Through an Orenda 8 Engine", Suffield TN No. 219.

2 Muirhead, J.C., "A Review of DRES Studies on the Effect of Blast on Gas Turbine Engines", Suffield Rept. No. 267.

3 Muirhead, J.C., Naylor, R. and Felt, G.D., "The Transmission of Blast Waves Through an Orenda 8 Engine from Exhaust to Inlet", Suffield Memo. 89/69.

4 Ludwig, G.R., "Tests of an Improved Rotating Stall Control System on a J-85 Turbojet Engine", AFAPL TR-79, May 1979.

5 Private Communication, R. Smiley and J.R. Ruetenik, Kaman AviDyne Corp., to M. Dunn, Calspan Corp., 2-3 November 1978.

6 Ludwig, G.R. and Arendt, R.H., "Investigation of Rotating Stall Phenomena in Axial Flow Compressors", Vol. III Development of a Rotating Stall Control System, AFAPL-TR-76-48, Vol. III, June 1976.

7 Jansen, W., Swarden, M.C. and Carlson, A.W., "Compressor Sensitivity to Transient and Distorted Transient Flows, Volume II-Mathematical Details and Computer Programs", Northern Research and Engineering Corporation, Cambridge, Mass., January 1971. AD728024

8 Curtis, J.T., Moselle, J.R. and Nenni, J.P., "One-Dimensional Analysis of Transient Compressor Performance", Calspan Corporation Rept. currently in preparation.

9 Sugiyama, Y., Hamed, A., and Tabakoff, W., "A Study of Compressor Surge Due to Inlet Pressure Disturbances", AIAA Paper 78-246, January 1978.

TABLE 1 EXPERIMENTAL CONDITIONS FOR WHICH DATA ARE AVAILABLE

% CORRECTED ENGINE SPEED	ΔP , PSI	OBSERVED COMPRESSOR CASING PEAK-PEAK VIBRATION, IN.
0	2.4	0.003
0	3.9	0.006
70	2.5	-
	3.3	0.003
	4.4	0.010
80	3.5	0.004
88	1.1	0.001
	2.3	0.003
93	1.0	0.001
93.7	2.2	0.003
94.3	3.3	0.005

NOTE: MACHINE IS RED-LINED AT 0.006 IN.

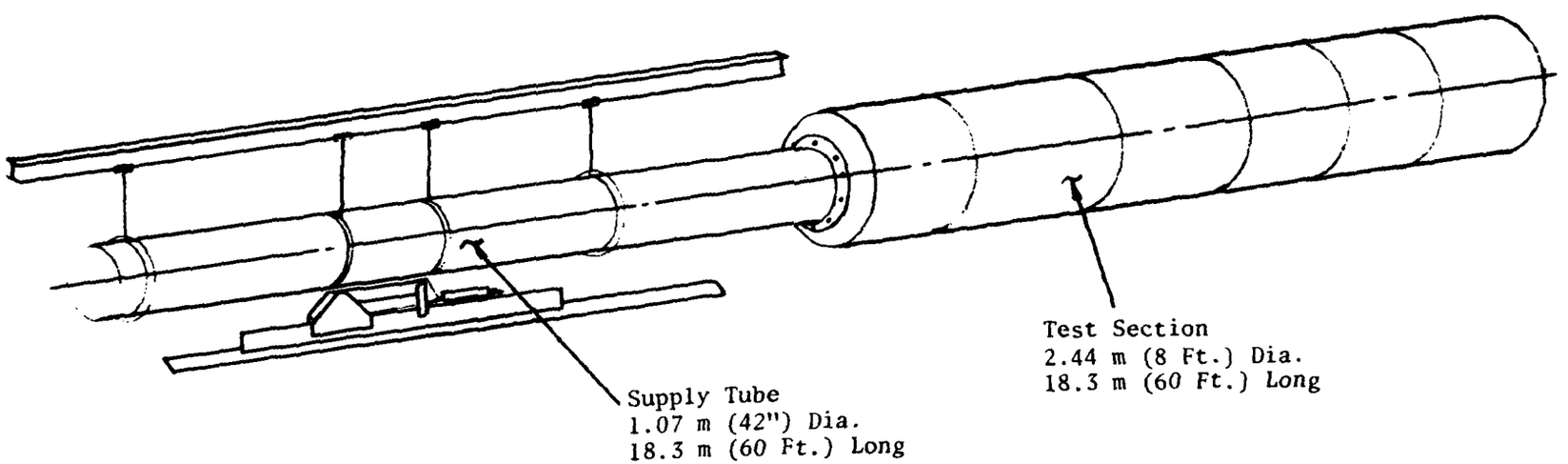

Figure 1 LUDWIEG-TUBE FACILITY

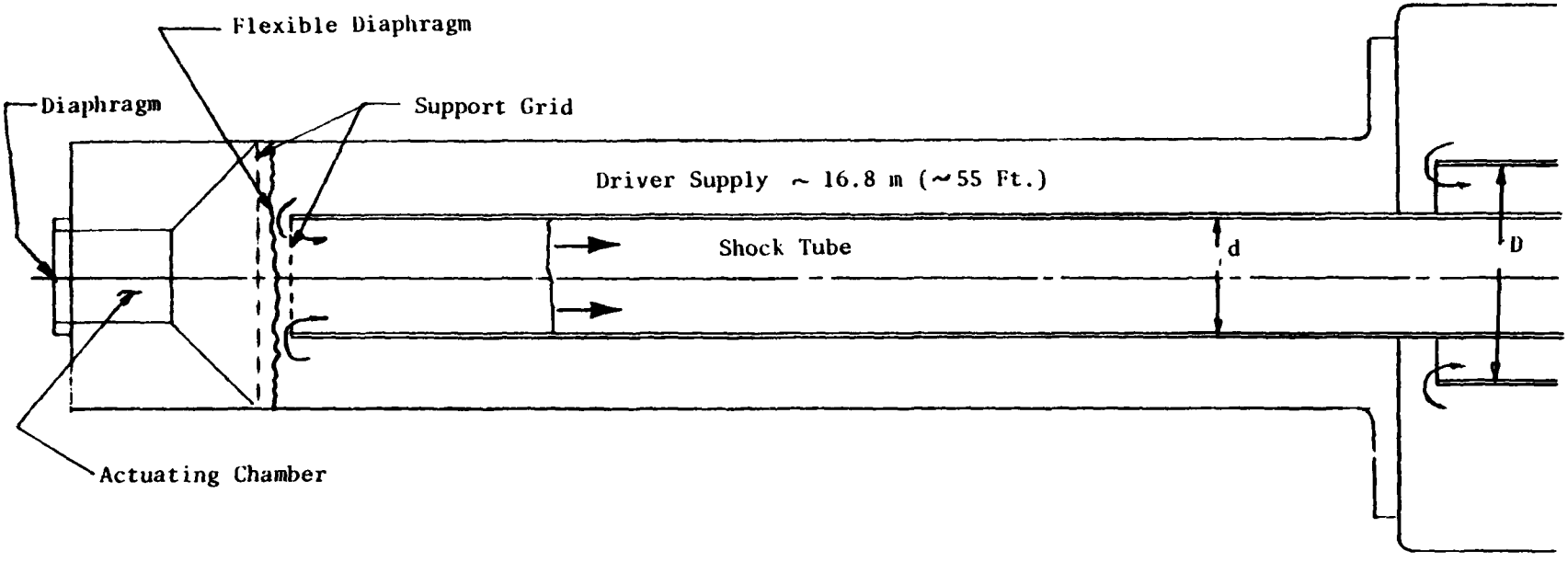

Figure 2 SKETCH OF SYSTEM

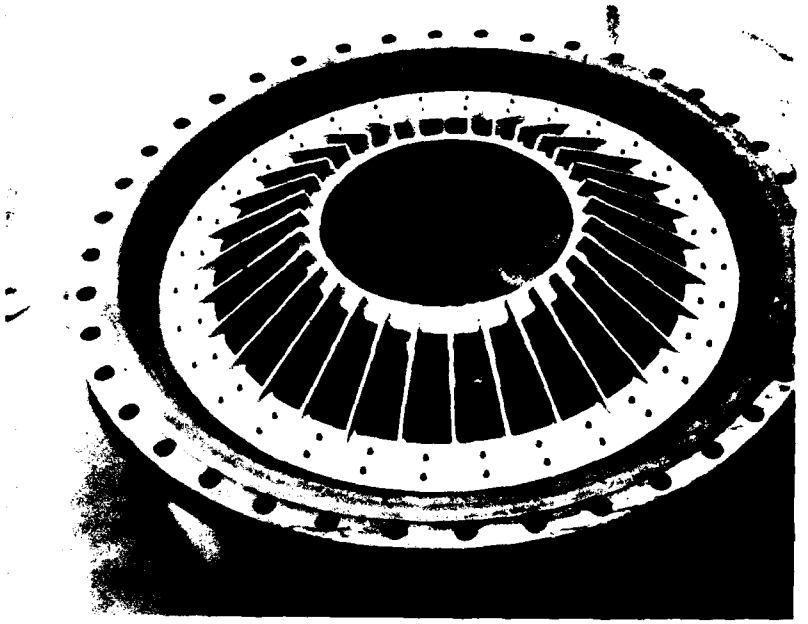

a) Neoprene Diaphragm

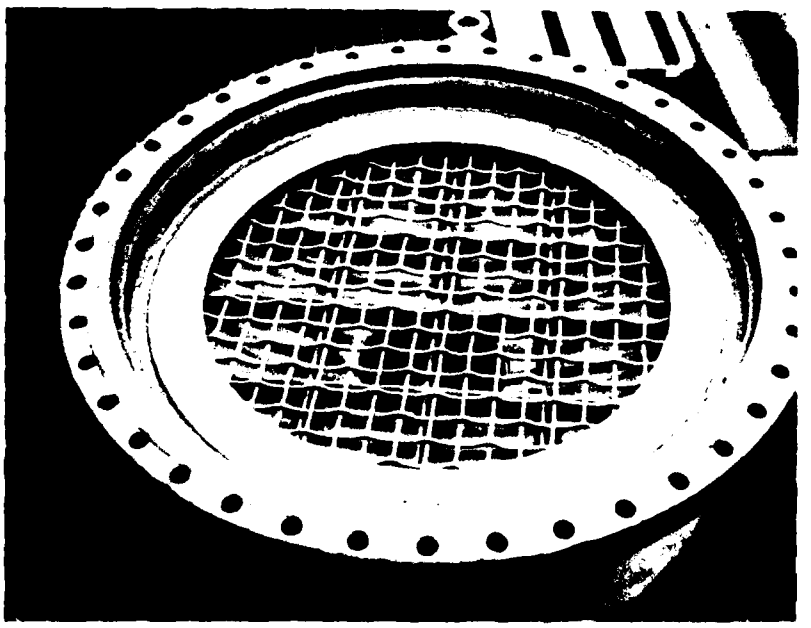

b) Back-up Grid for Diaphragm

Figure 3 PHOTOGRAPH OF ACTUATING CHAMBER

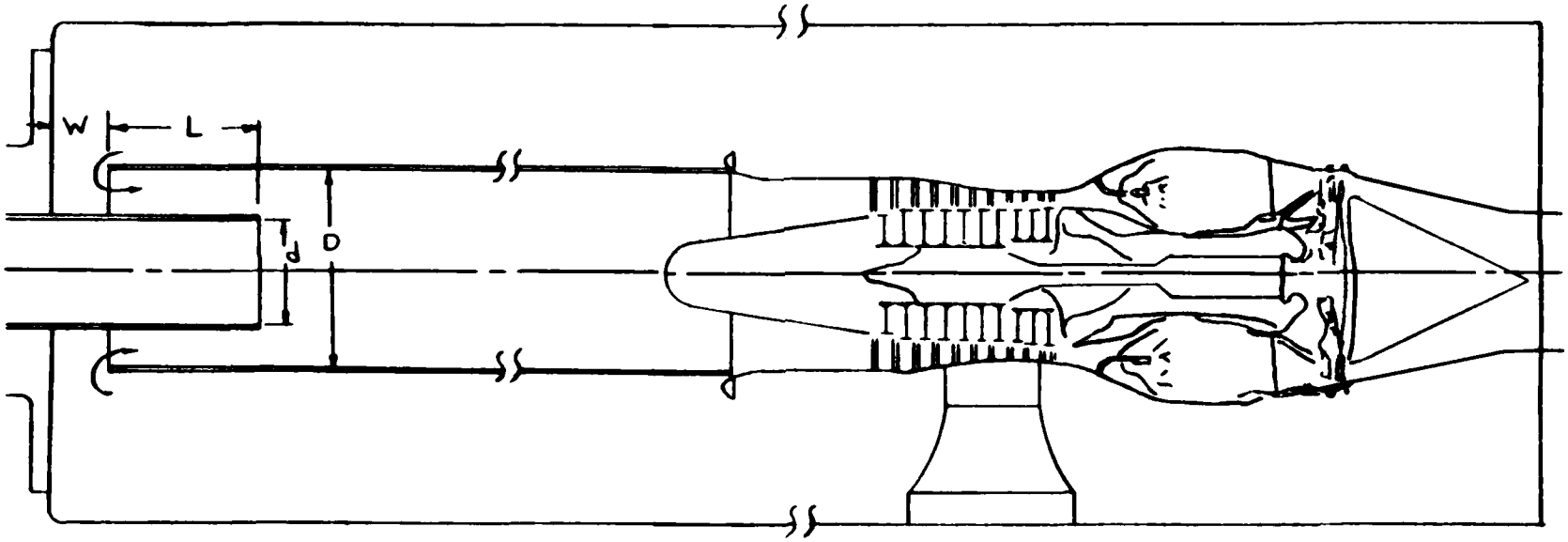

Figure 4 SKETCH OF ENGINE IN TEST SECTION

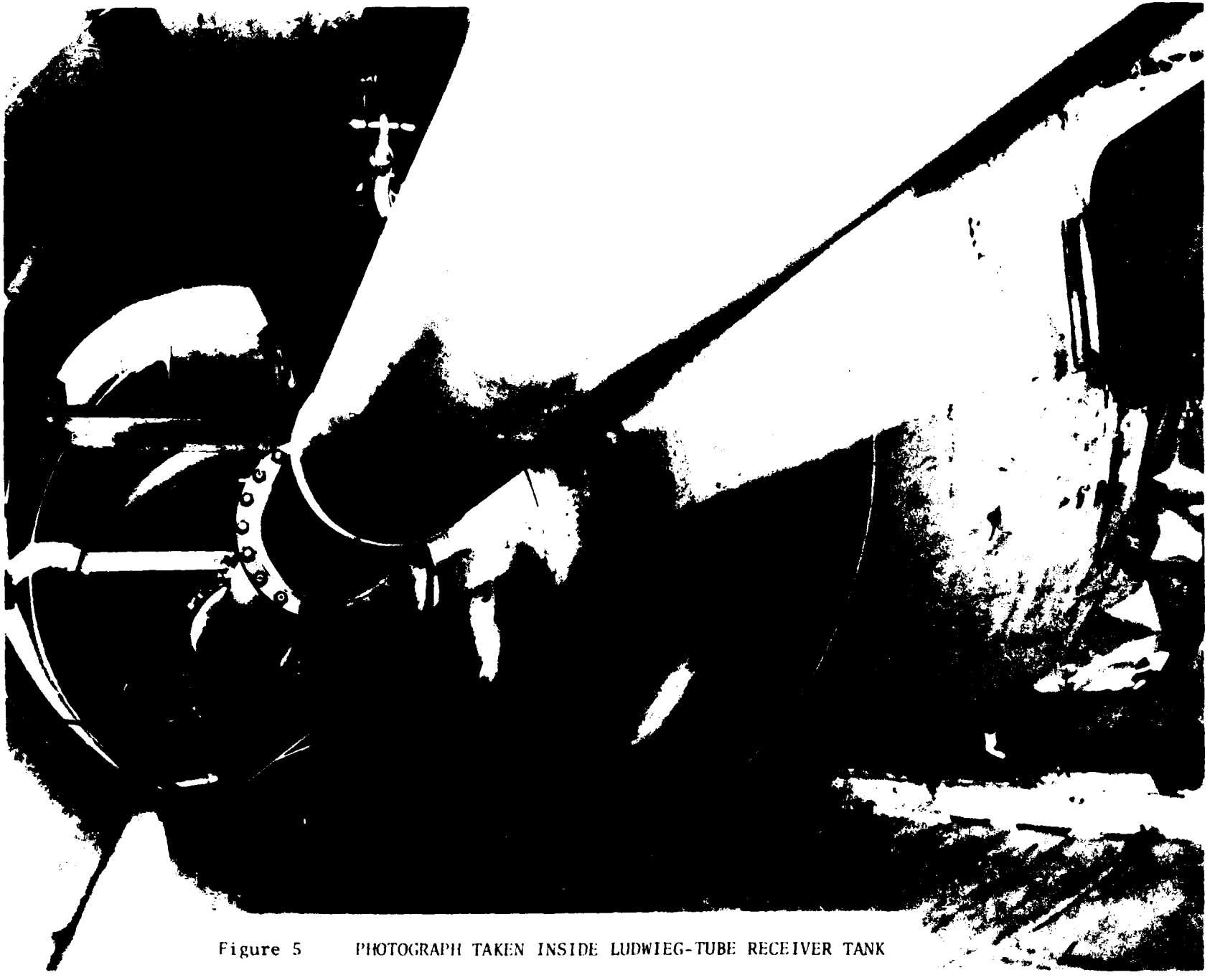

Figure 5 PHOTOGRAPH TAKEN INSIDE LUDWIEG-TUBE RECEIVER TANK

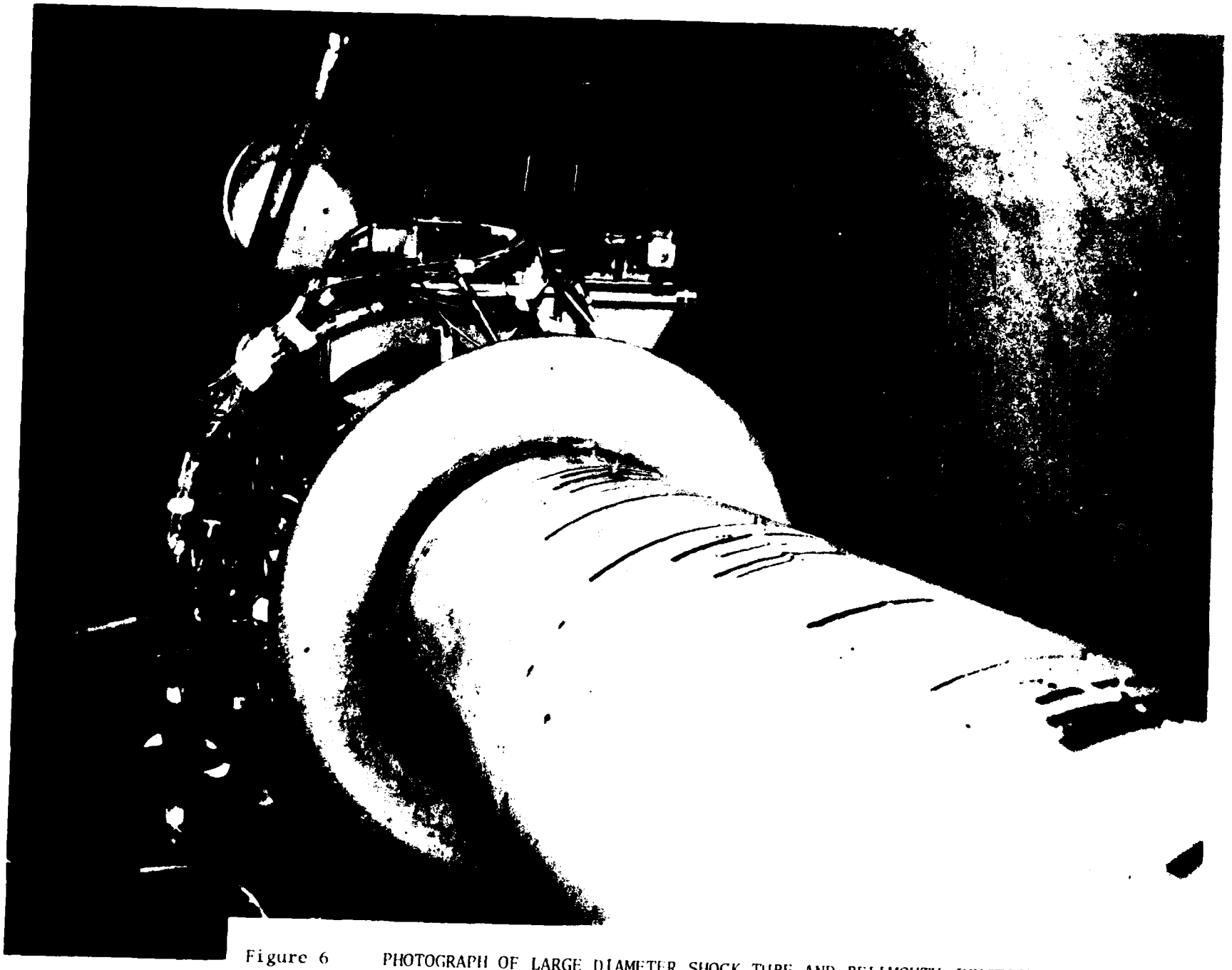

Figure 6 PHOTOGRAPH OF LARGE DIAMETER SHOCK TUBE AND BELLMOUTH JUNCTION

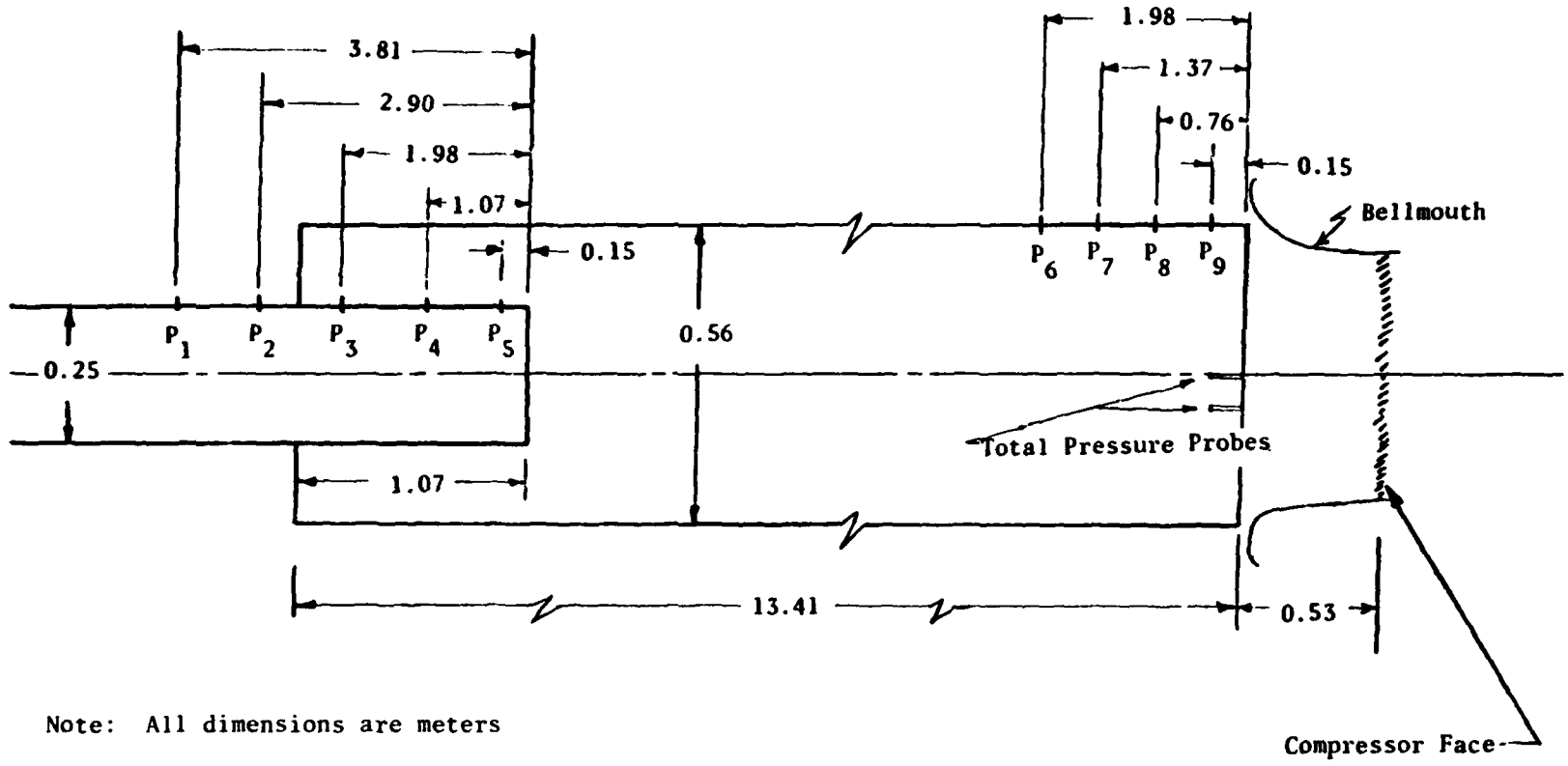

Note: All dimensions are meters

Figure 7 SKETCH OF SHOCK-TUBE INSTRUMENTATION

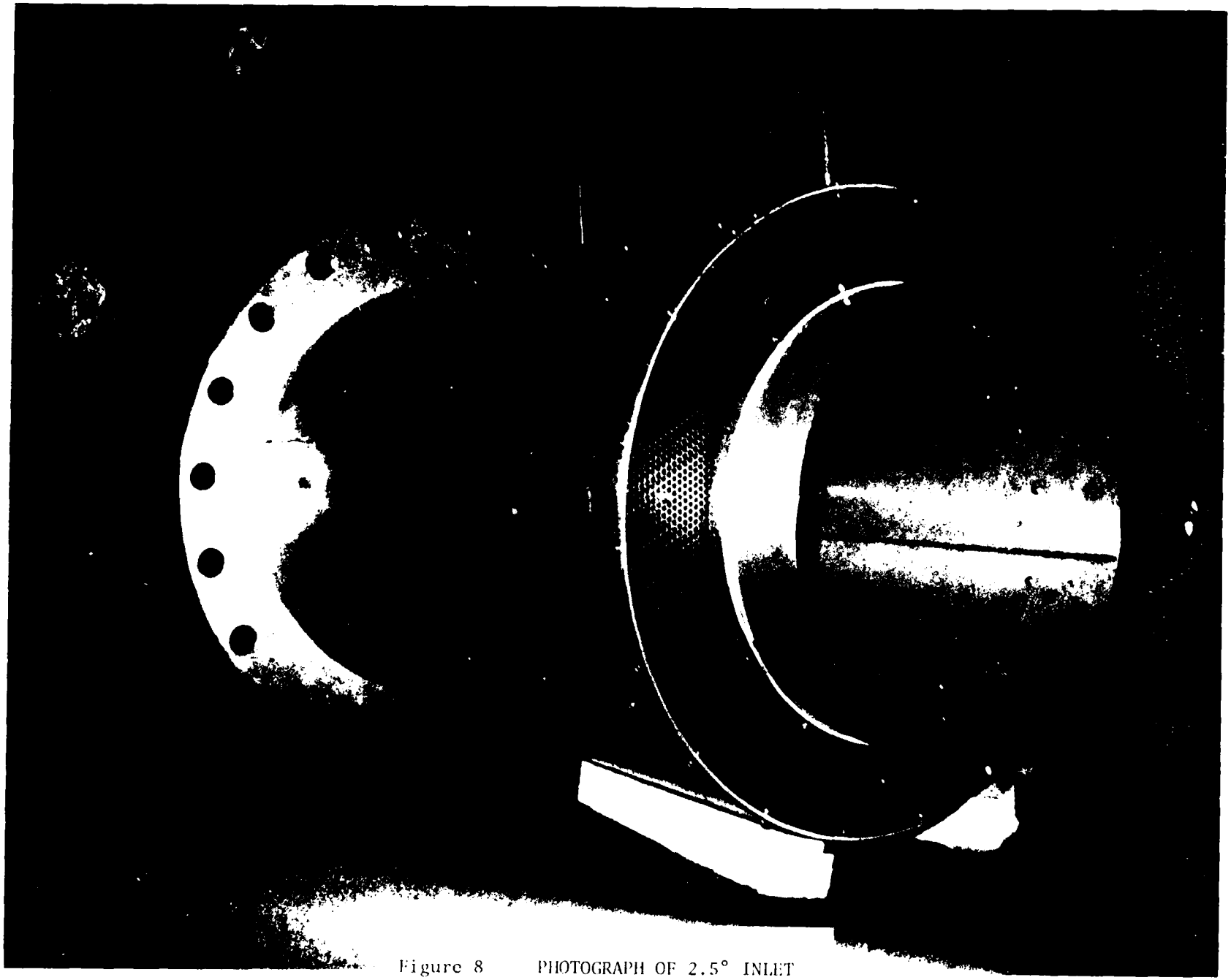

Figure 8 PHOTOGRAPH OF 2.5° INLET

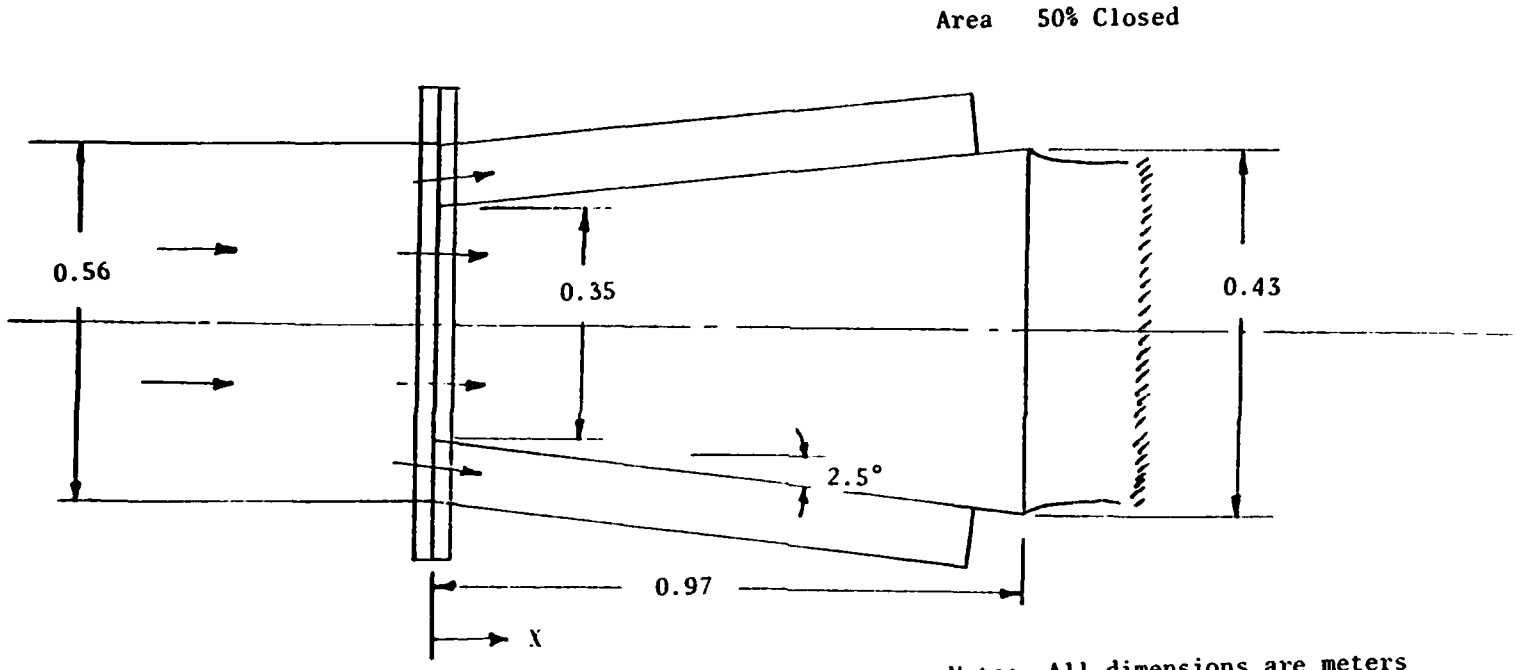

Note: All dimensions are meters

Pressure Transducers at:

X = 0.10, 0.20, 0.30, 0.41, 0.51, 0.51, 0.61, 0.71,

0.81, 0.91, 0.94 meters

Figure 9 SKETCH OF CONFIGURATION USED FOR INLET EXPERIMENTS

Left Side

Right Side

Figure 10 PRESSURE TRANSDUCER LOCATIONS IN FORWARD PORTION OF J-85 COMPRESSOR

Left Side Installation

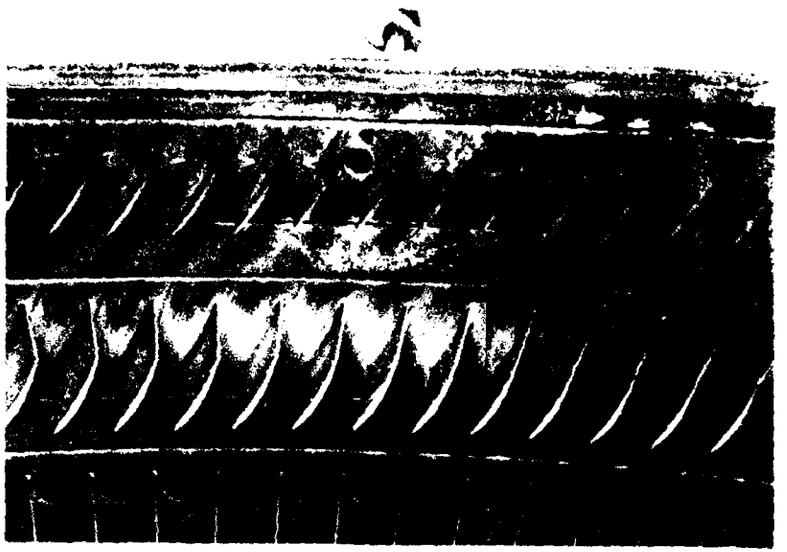

Upper Installation

Figure 11 PRESSURE TRANSDUCER LOCATIONS IN REAR OF J-85 COMPRESSOR

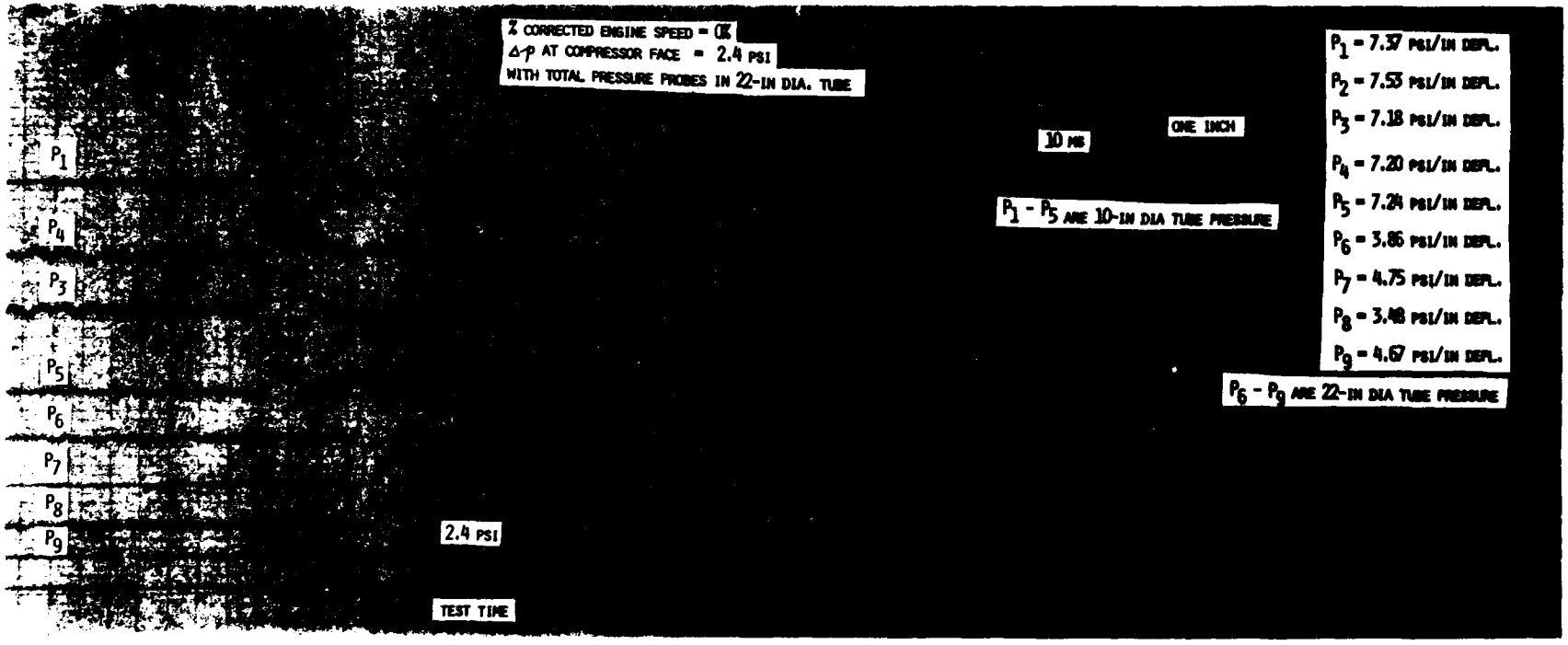

Figure 12 (a) SHOCK-TUBE PRESSURE HISTORIES FOR Δp = 2.4 psi WITH ENGINE AT REST

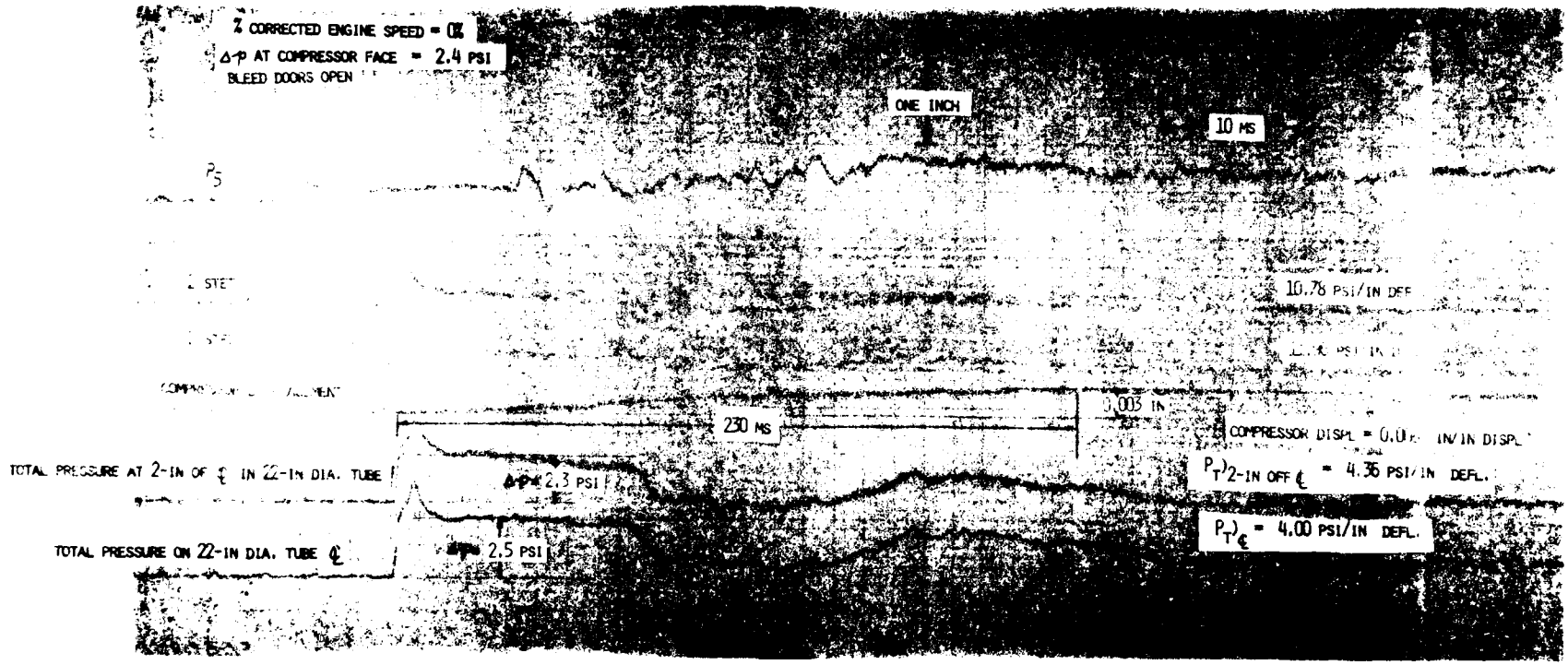

Figure 12 (b) TOTAL PRESSURE MEASUREMENTS IN SHOCK TUBE WITH ENGINE AT REST

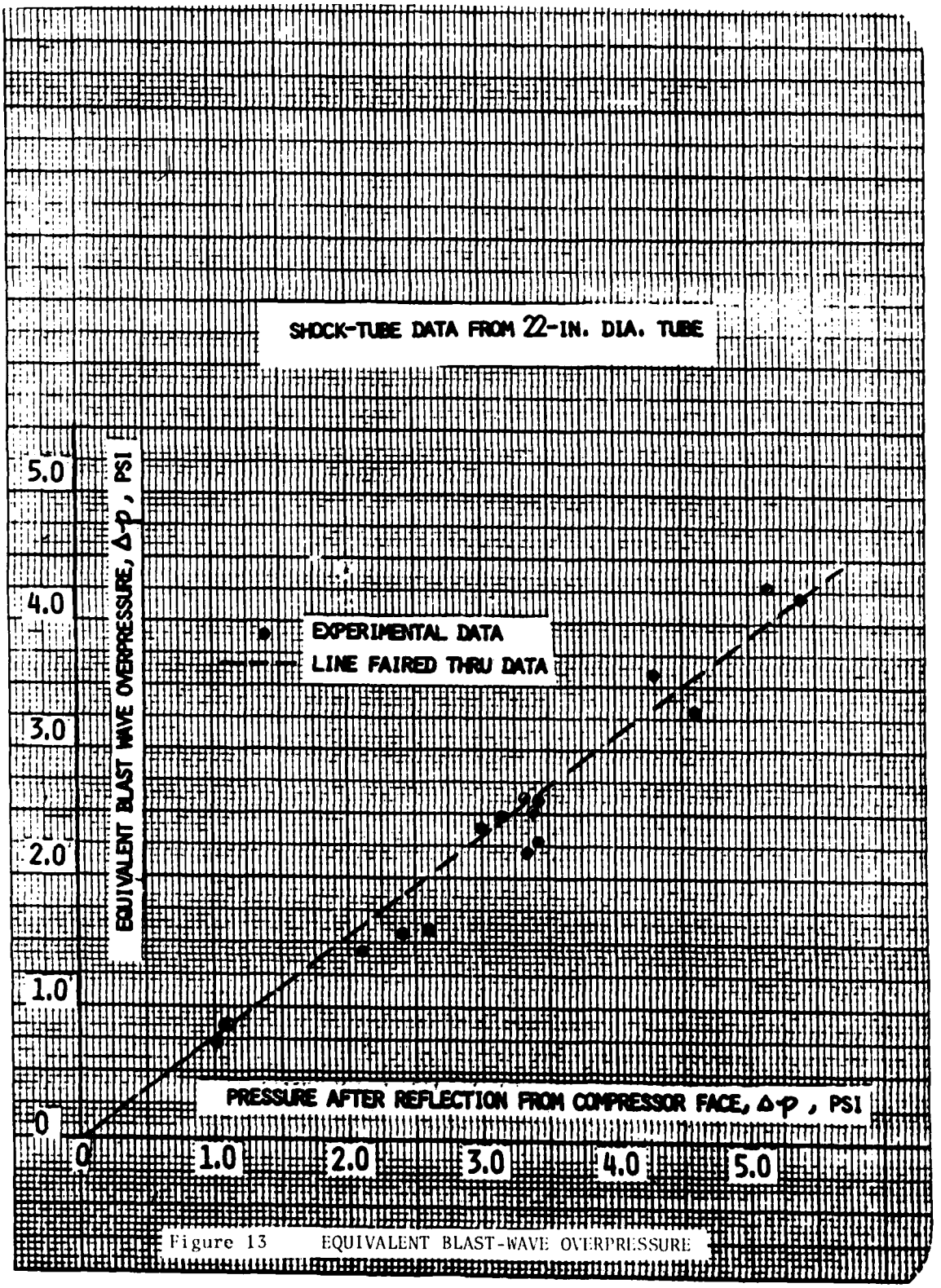

Figure 13 EQUIVALENT BLAST-WAVE OVERPRESSURE

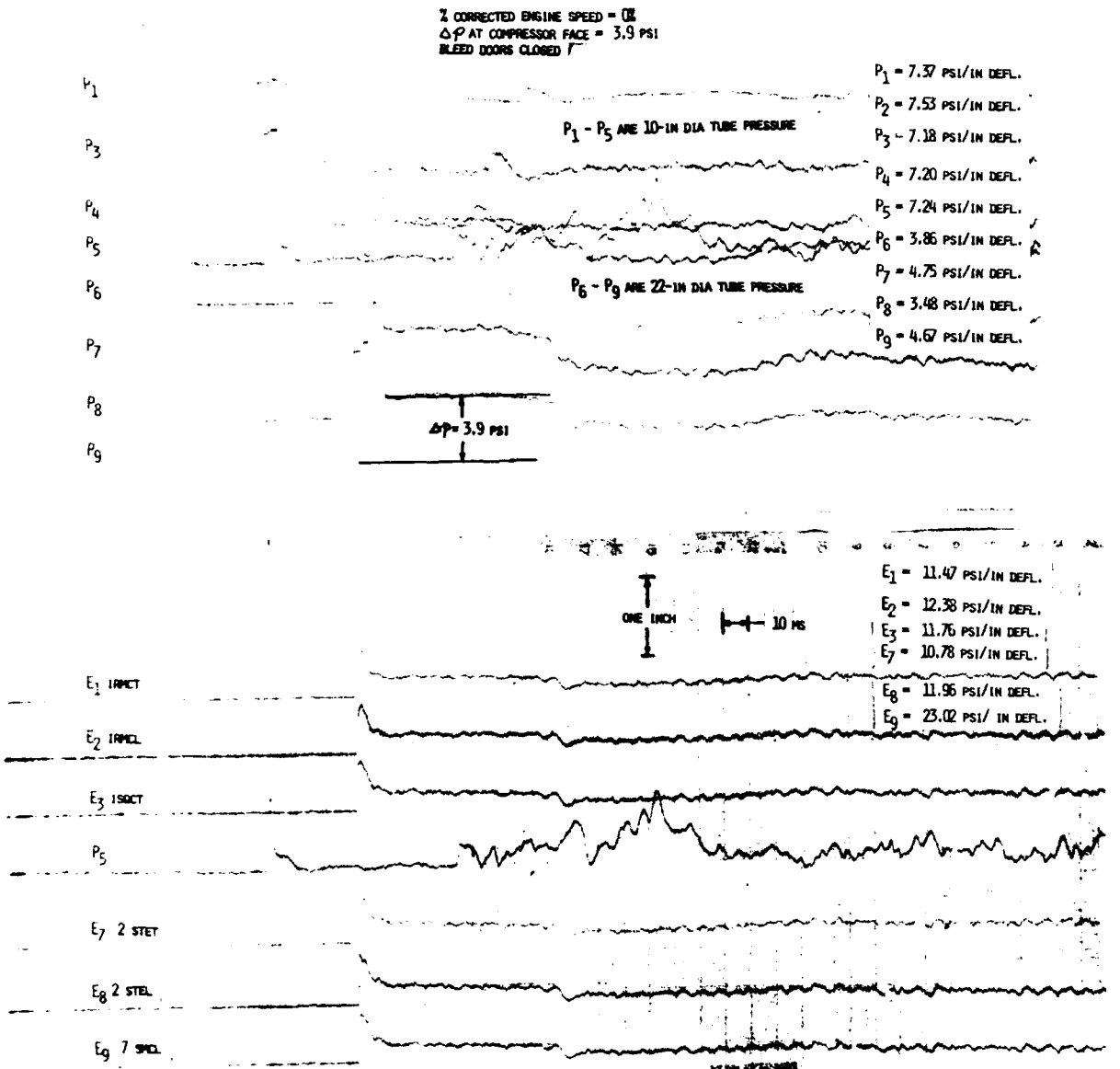

Figure 14 (a) SHOCK-TUBE AND ENGINE PRESSURE HISTORIES FOR ΔP = 3.9 psi SHOCK WAVE WITH ENGINE AT REST

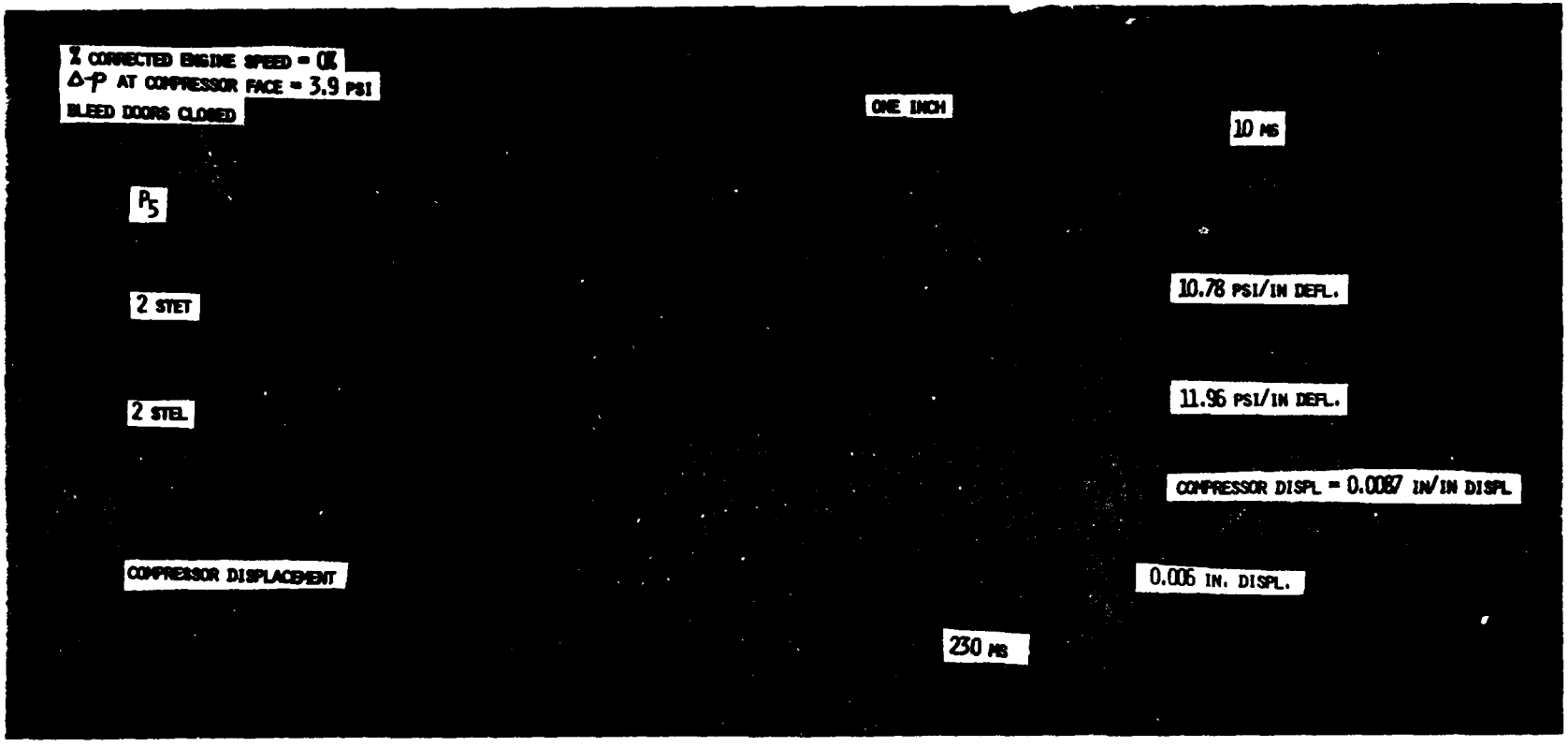

Figure 14 (b) ENGINE PRESSURE AND COMPRESSOR CASING DISPLACEMENT HISTORIES FOR Δp = 3.9 psi SHOCK WAVE WITH ENGINE AT REST

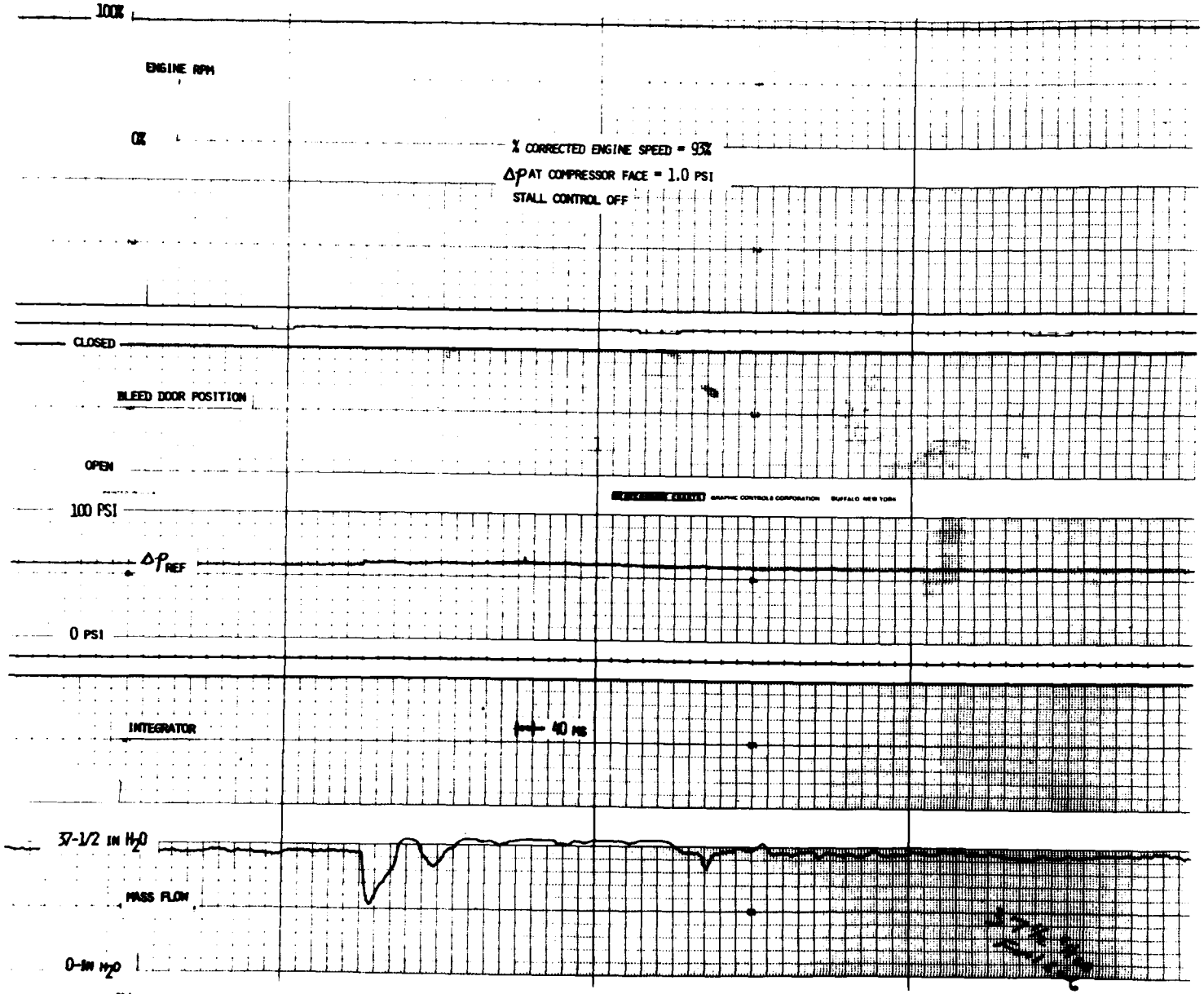

Figure 15 (a) TYPICAL HISTORY OF ENGINE PARAMETERS FOR ΔP = 1.0 psi SHOCK WAVE

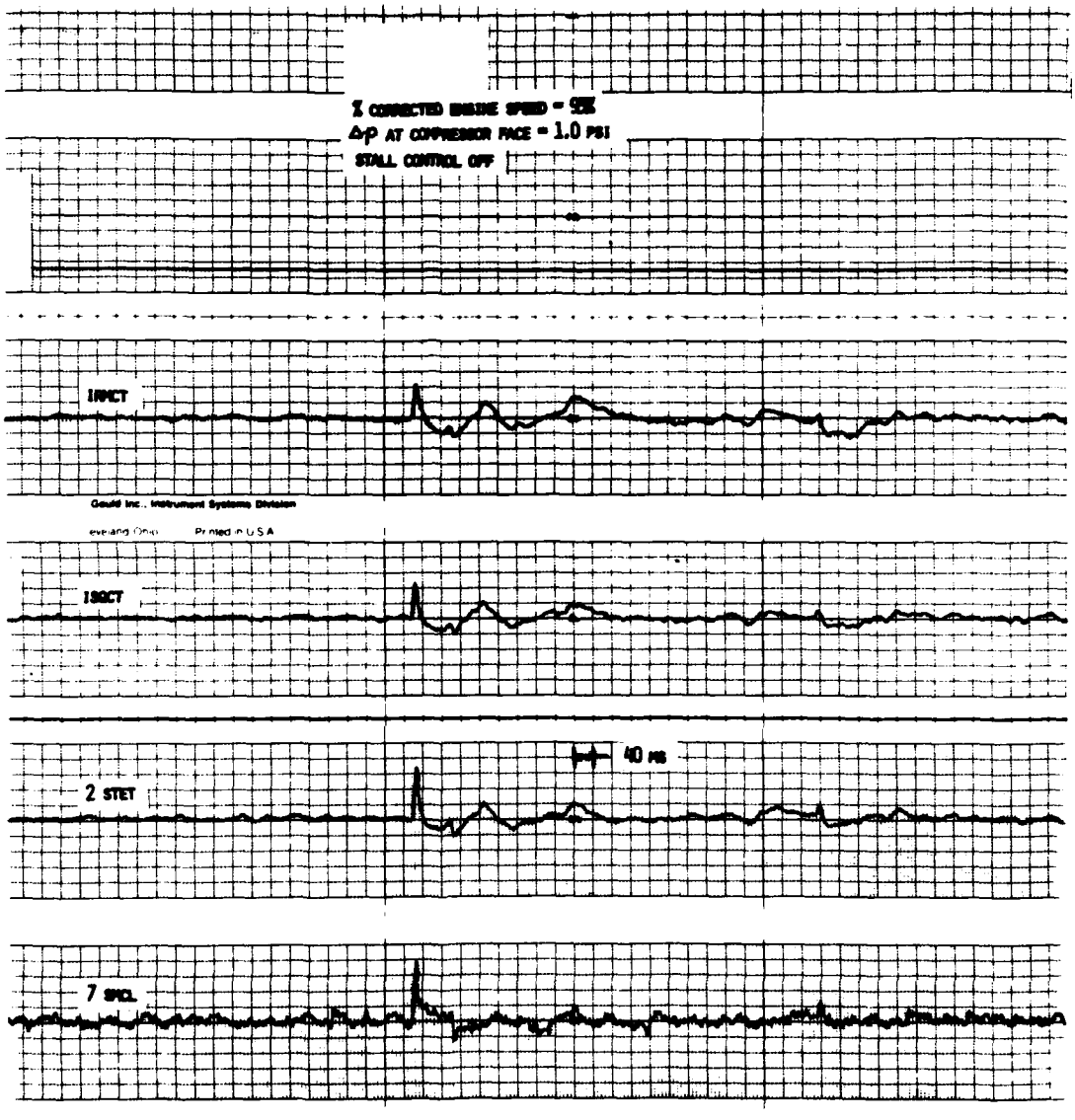

Figure 15 (b) SELECTED ENGINE PRESSURE HISTORIES FOR ΔP = 1.0 psi SHOCK WAVE

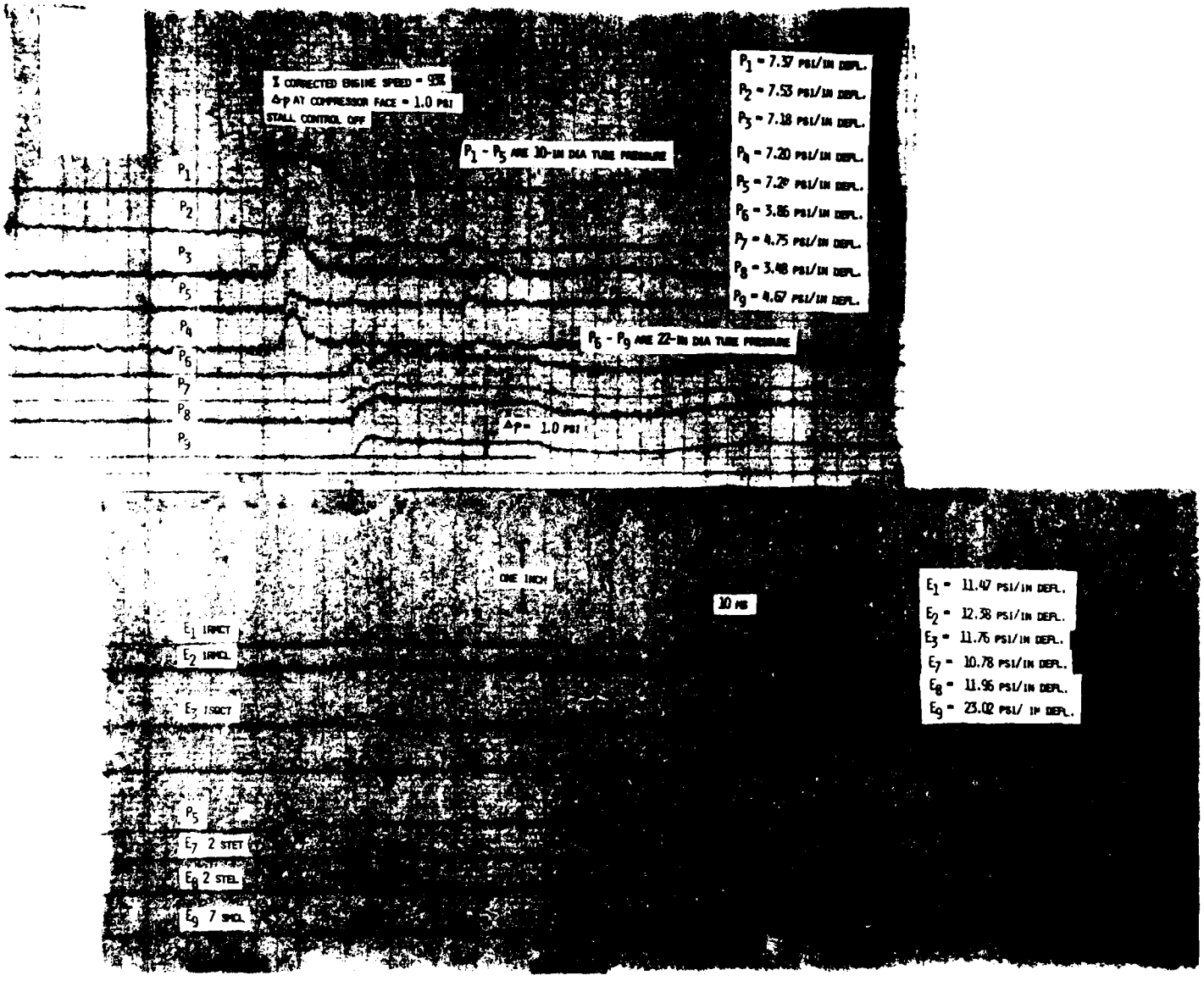

Figure 15 (c). SHOCK-TUBE AND ENGINE PRESSURE HISTORIES FOR ΔP = 1.0 psi SHOCK WAVE

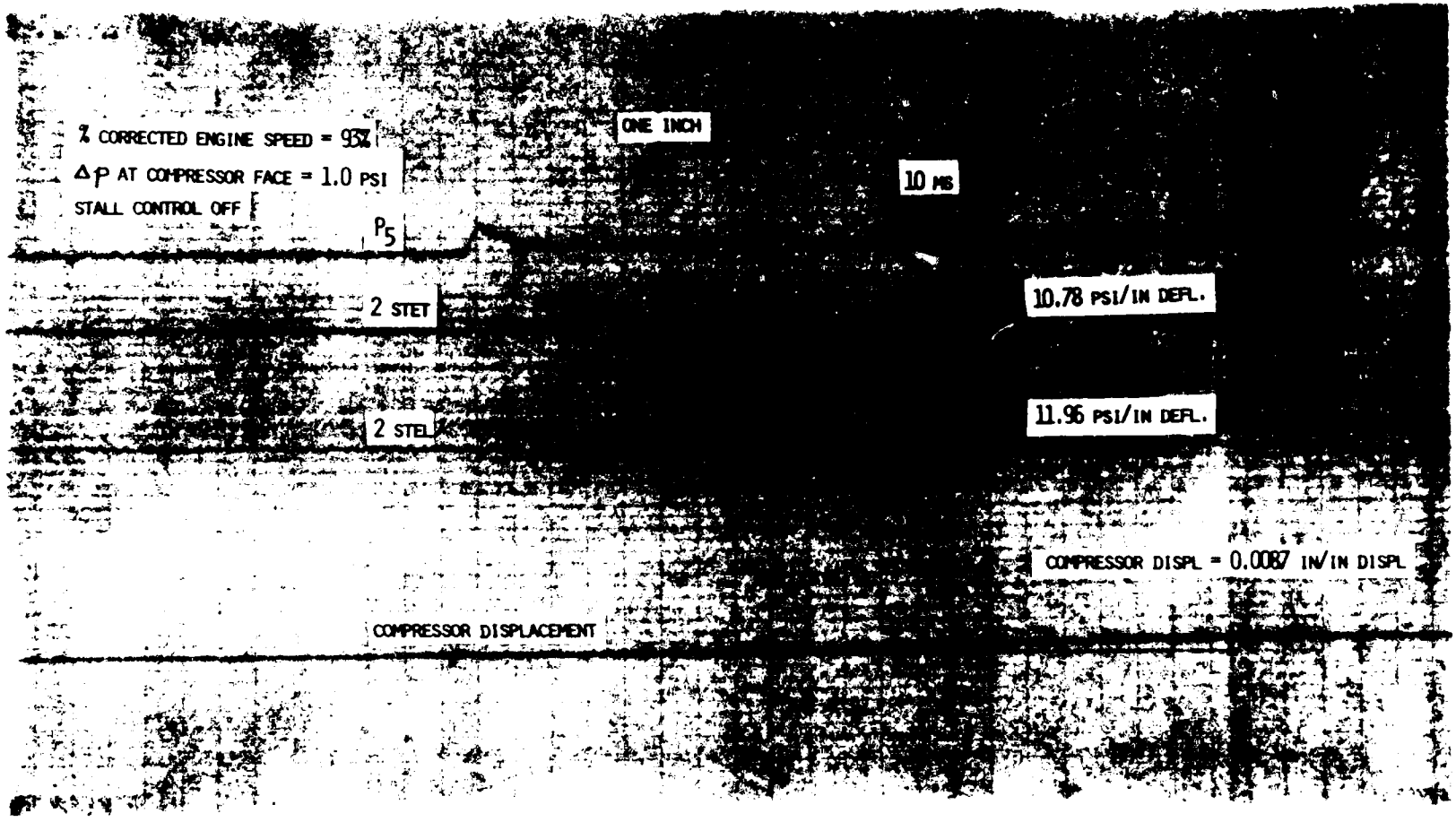

Figure 15 (d) SELECTED ENGINE PRESSURE HISTORIES FOR ΔP = 1.0 psi SHOCK WAVE

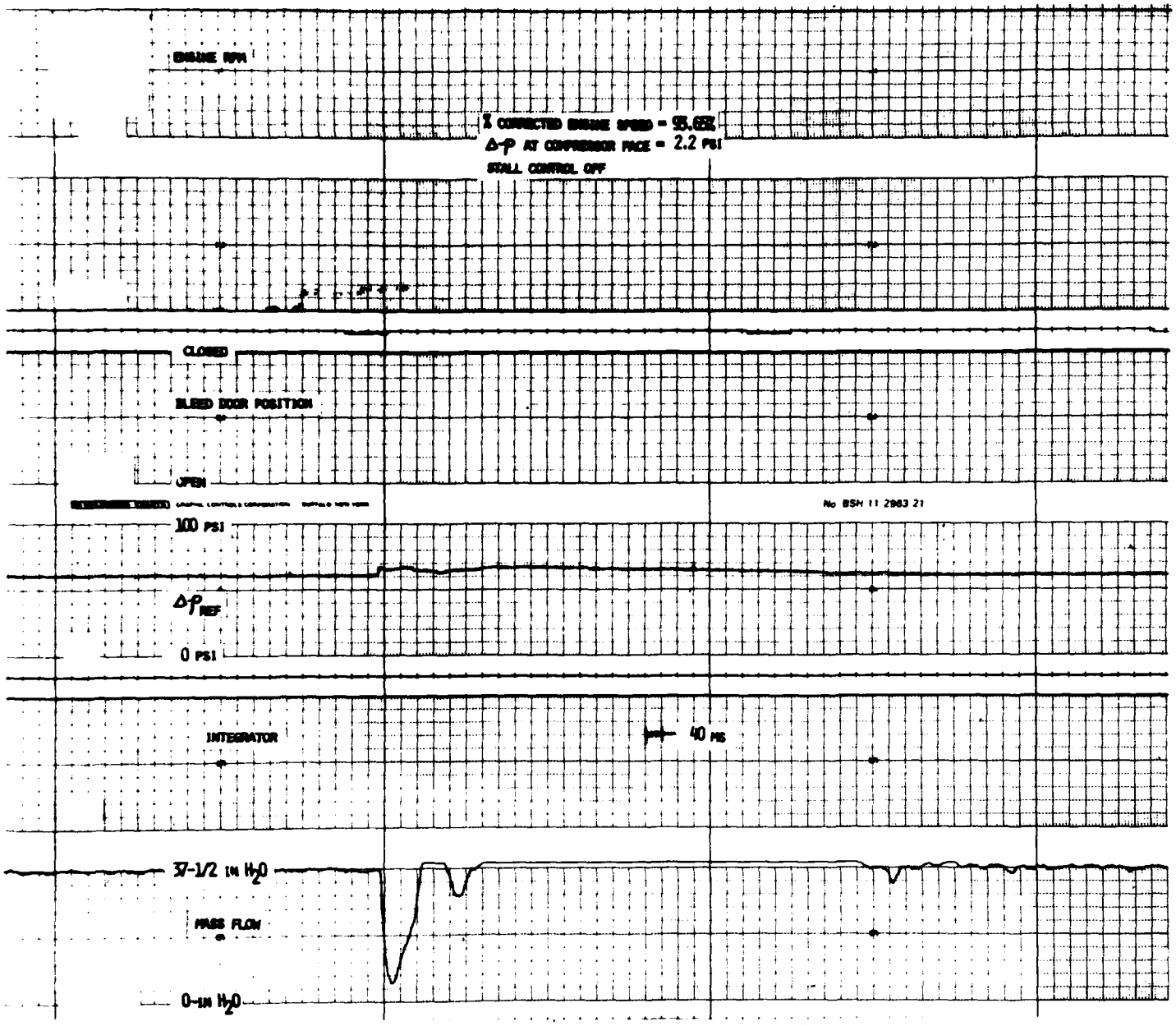

Figure 16 (a) TYPICAL HISTORY OF ENGINE PARAMETERS FOR ΔP = 2.2 psi SHOCK WAVE

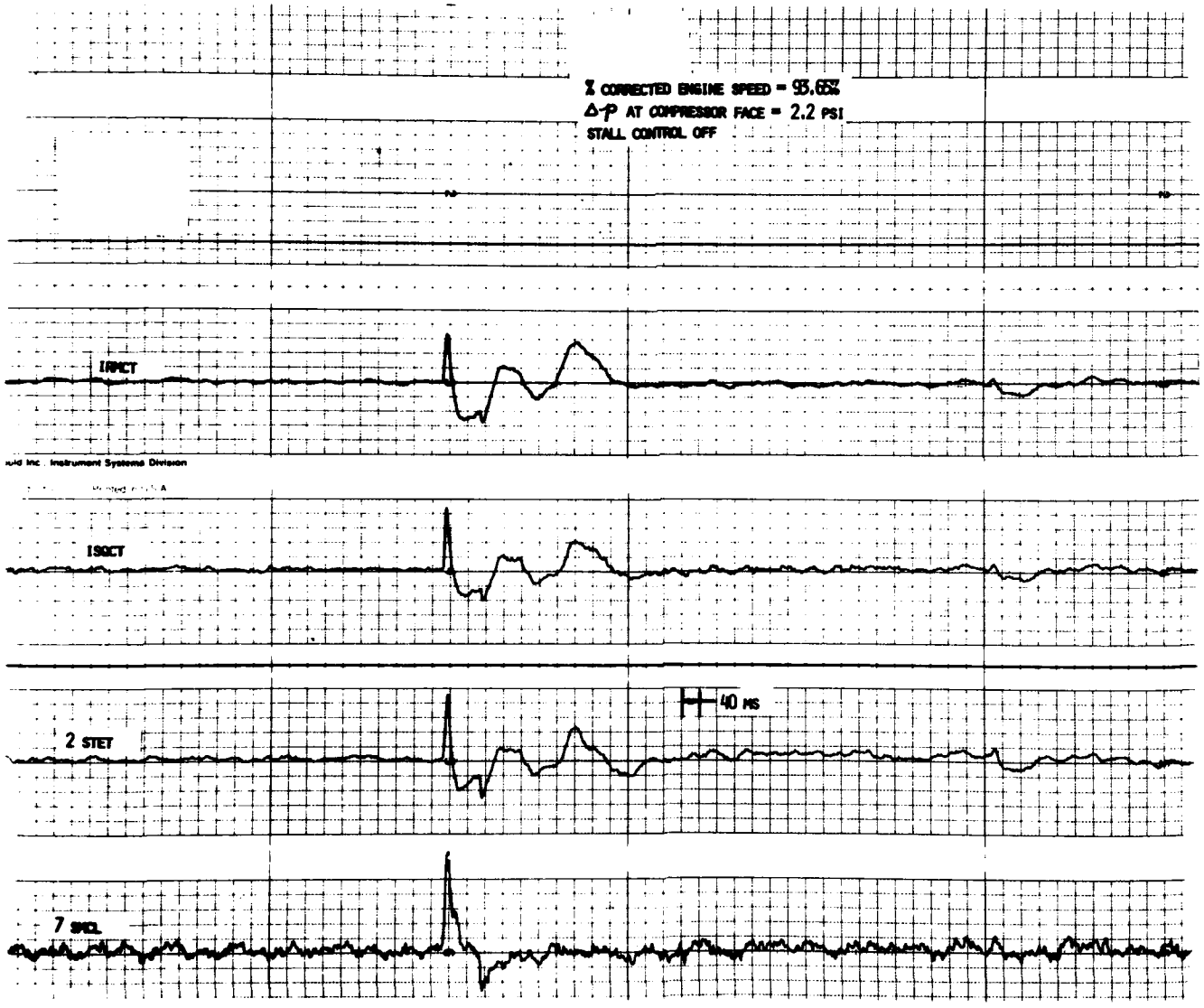

Figure 16 (b) SELECTED ENGINE PRESSURE HISTORIES FOR ΔP = 2.2 psi SHOCK WAVE

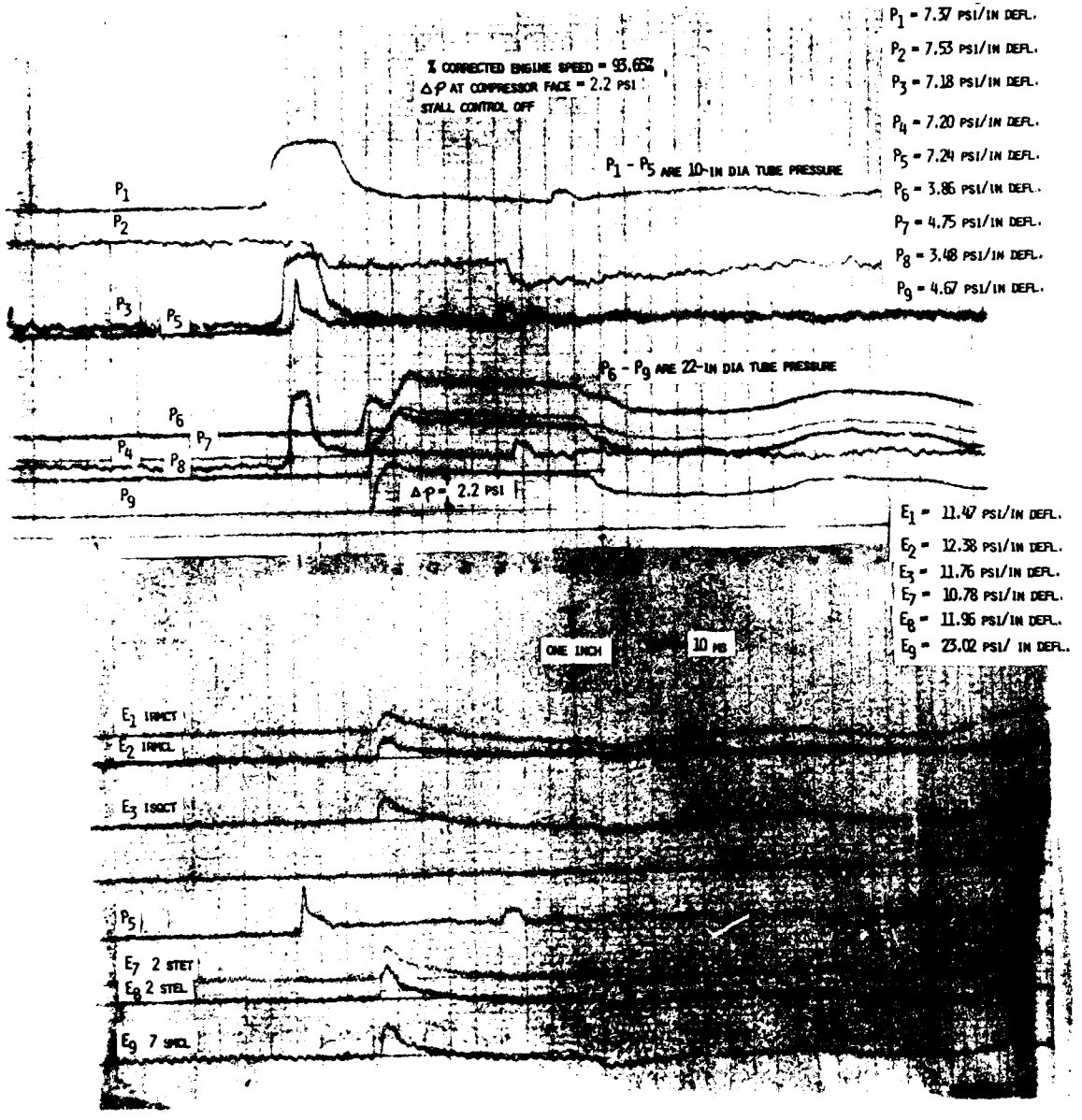

Figure 16 (c) SHOCK-TUBE AND ENGINE PRESSURE HISTORIES FOR ΔP = 2.2 psi SHOCK WAVE

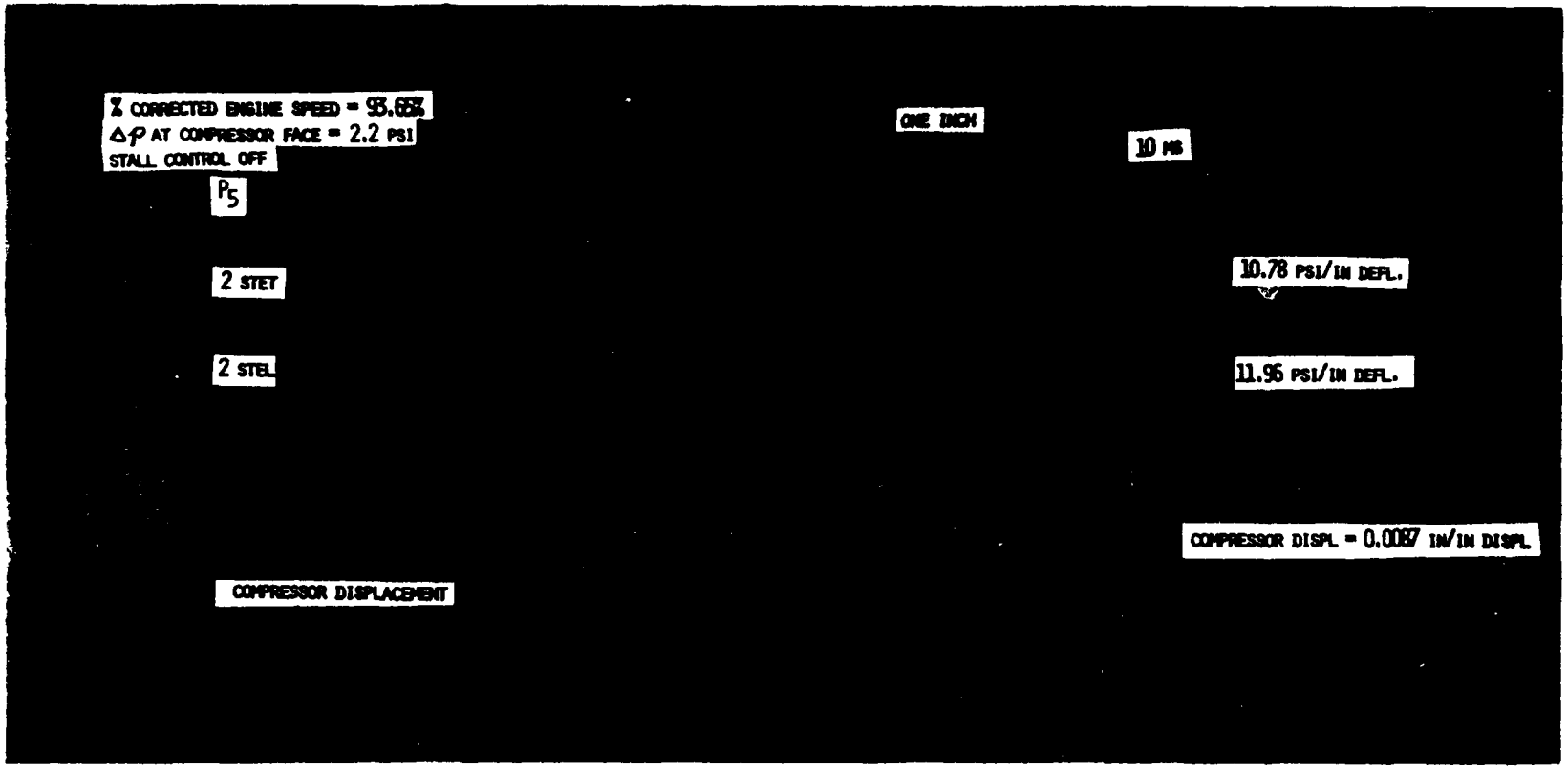

Figure 16 (d) SELECTED ENGINE PRESSURE HISTORIES FOR ΔP = 2.2 psi SHOCK WAVE

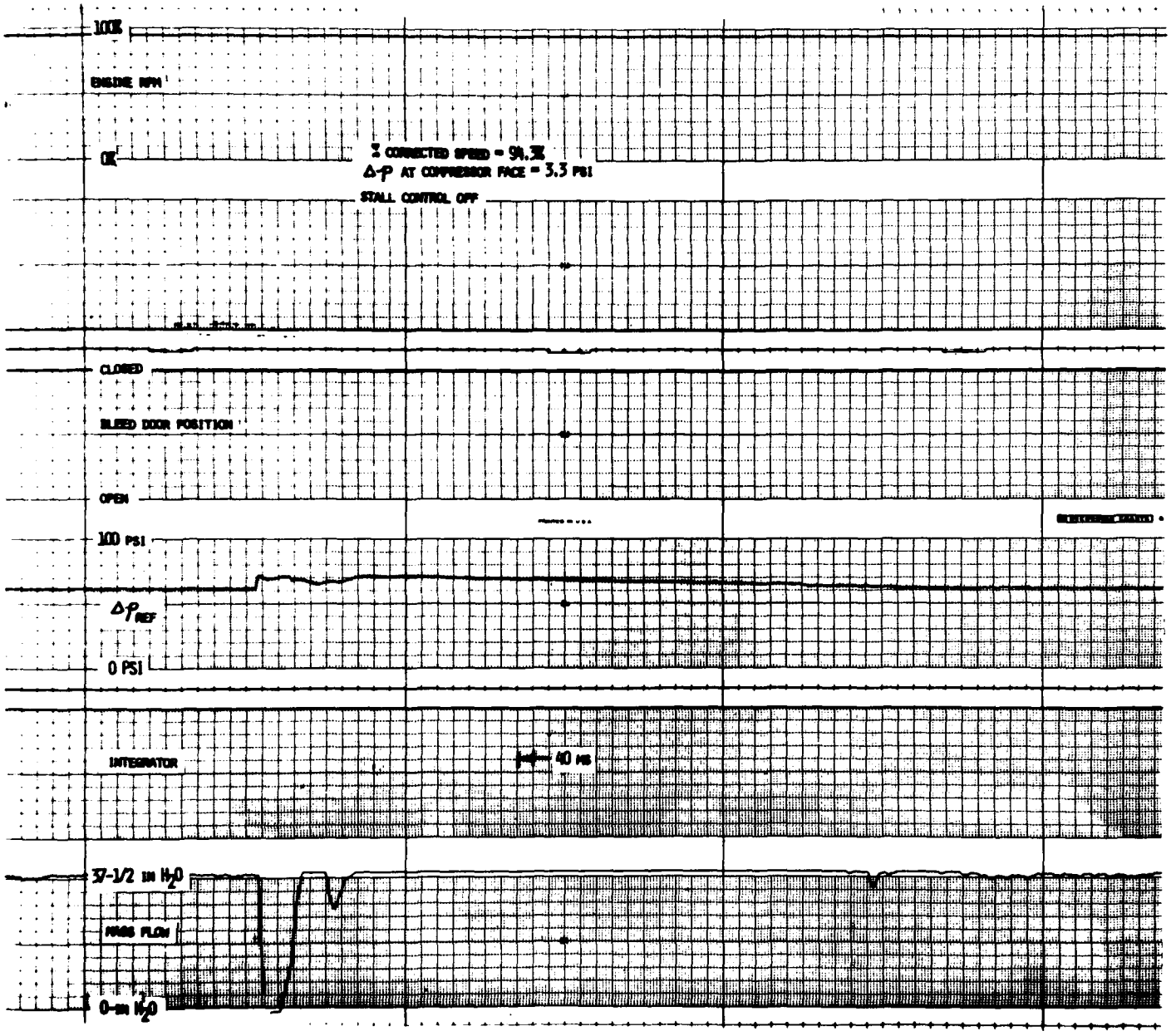

Figure 17 (a) TYPICAL HISTORY OF ENGINE PARAMETERS FOR ΔP = 3.3 psi SHOCK WAVE

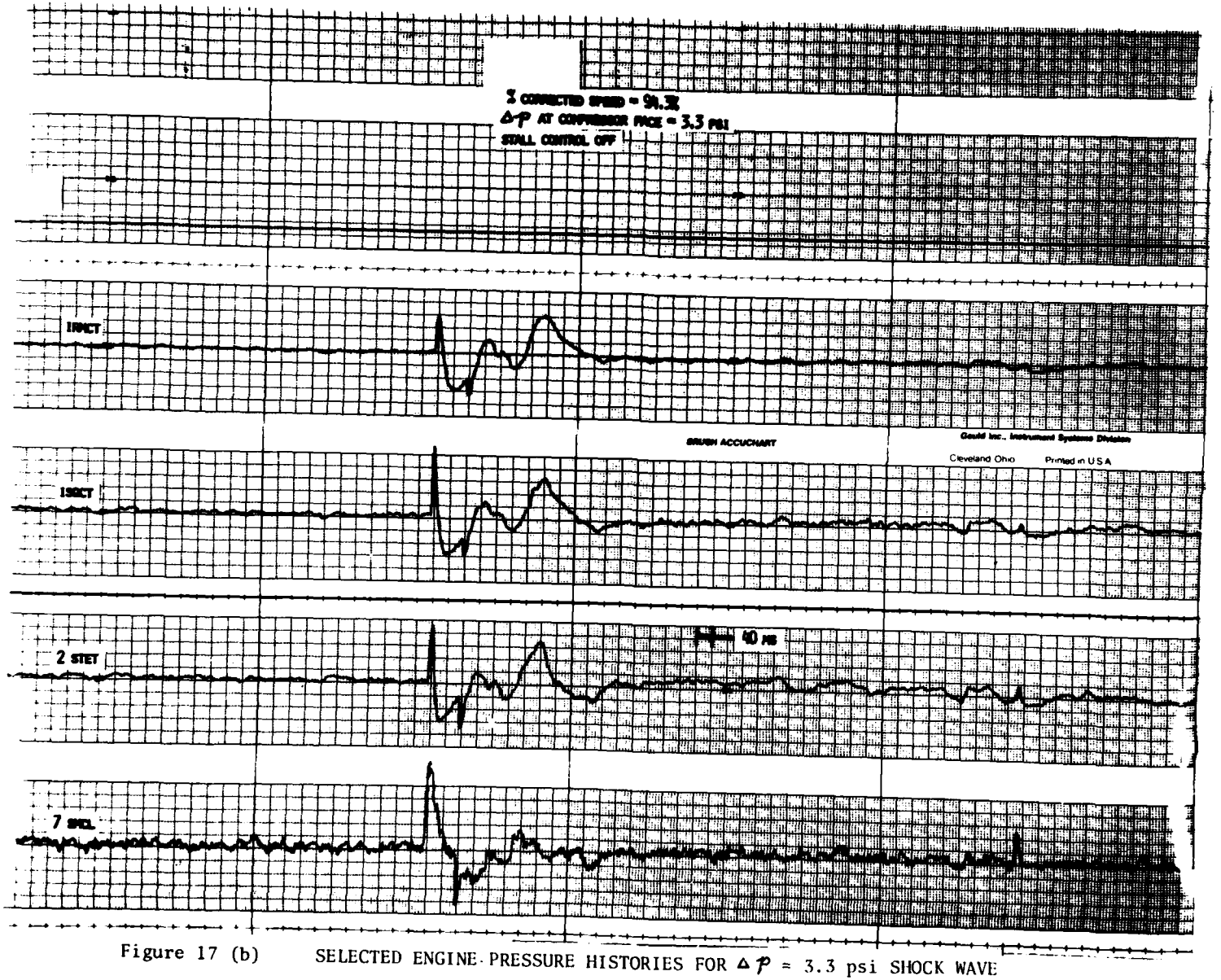

Figure 17 (b) SELECTED ENGINE PRESSURE HISTORIES FOR Δp = 3.3 psi SHOCK WAVE

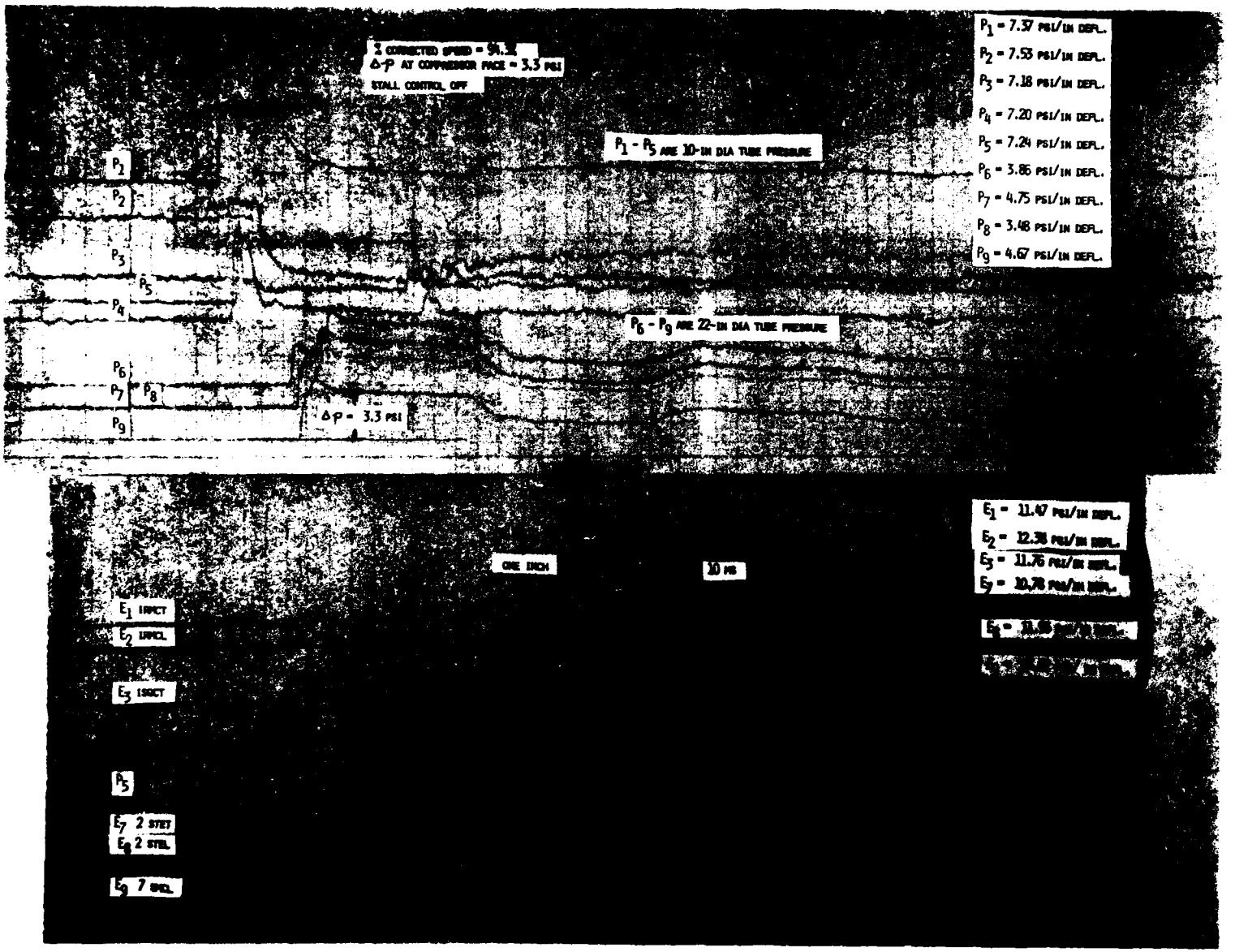

Figure 17 (c) SHOCK-TUBE AND ENGINE PRESSURE HISTORIES FOR ΔP = 3.3 psi

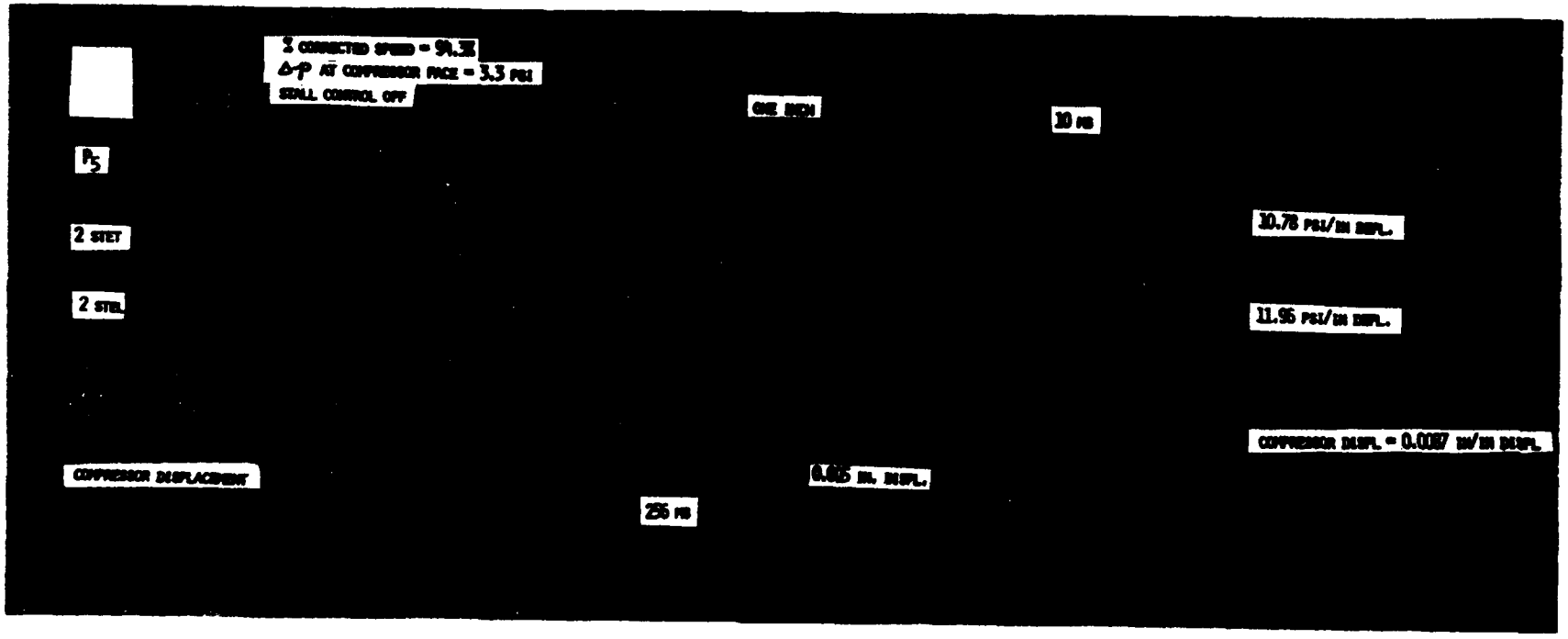

Figure 17 (d) SELECTED ENGINE PRESSURE HISTORIES FOR ΔP = 3.3 psi

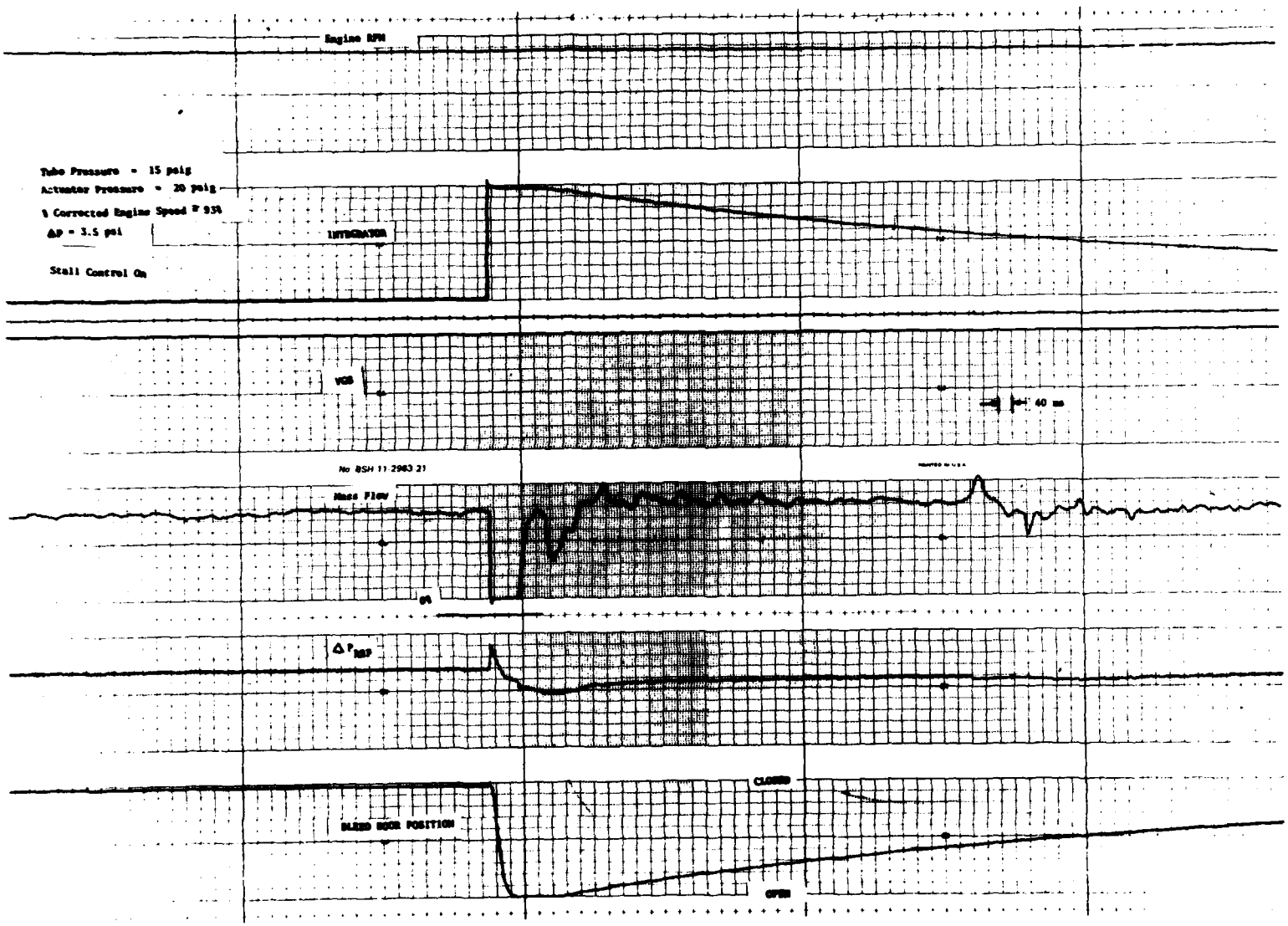

Figure 18 (a) TYPICAL HISTORY OF SHOCK-TUBE AND ENGINE PRESSURES FOR Δp = 3.5 psi WITH STALL CONTROL SYSTEM ACTIVE

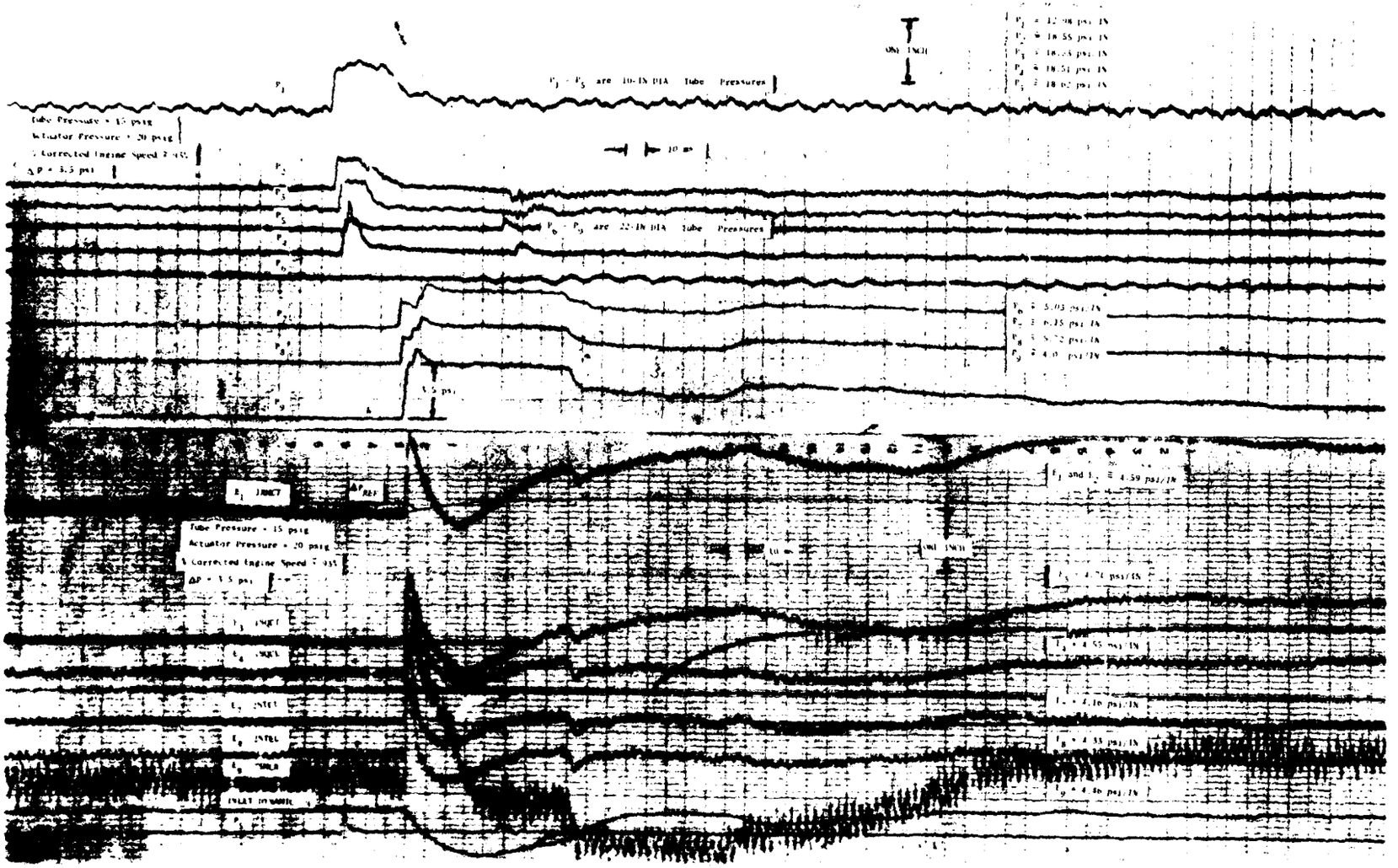

Figure 18 (b) TYPICAL HISTORY OF ENGINE PARAMETERS FOR ΔP = 3.5 psi WITH STALL CONTROL SYSTEM ACTIVE

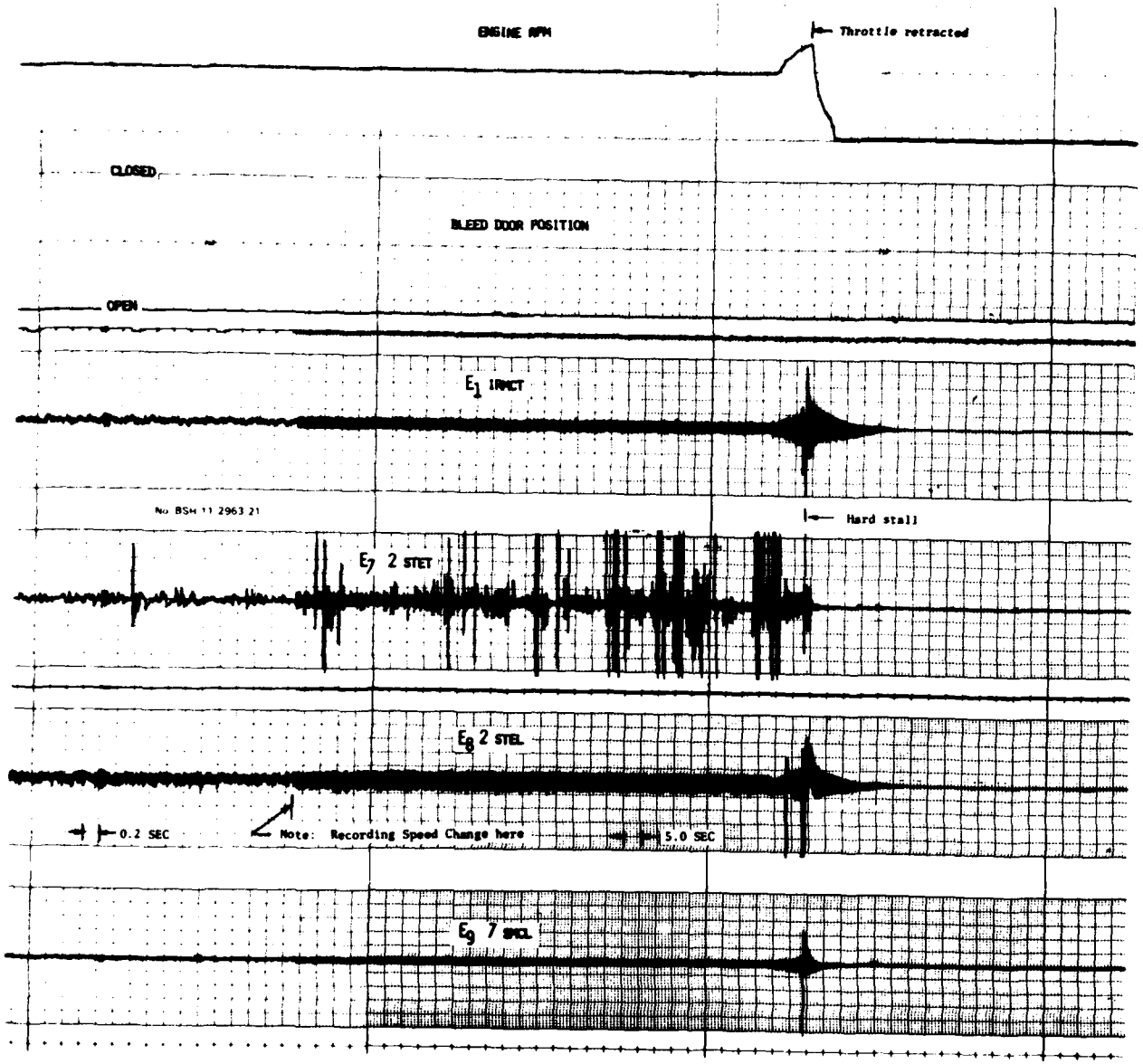

Figure 19 ENGINE PRESSURE HISTORIES WITH 2.5° HALF-ANGLE INLET INSTALLED

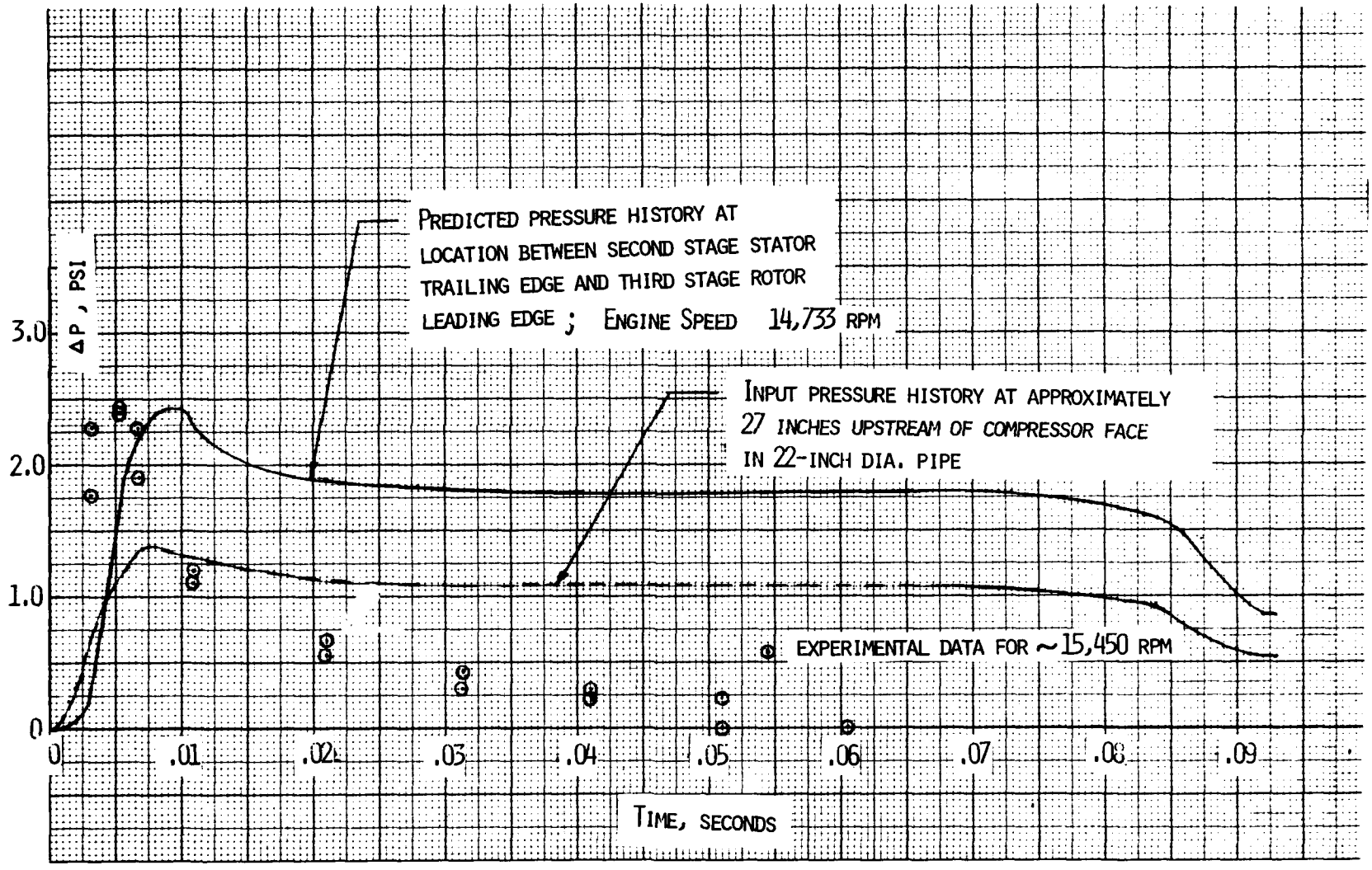

Figure 20 PRESSURE RESPONSE WITHIN J-85 COMPRESSOR FOR Δp = 1.1 psi

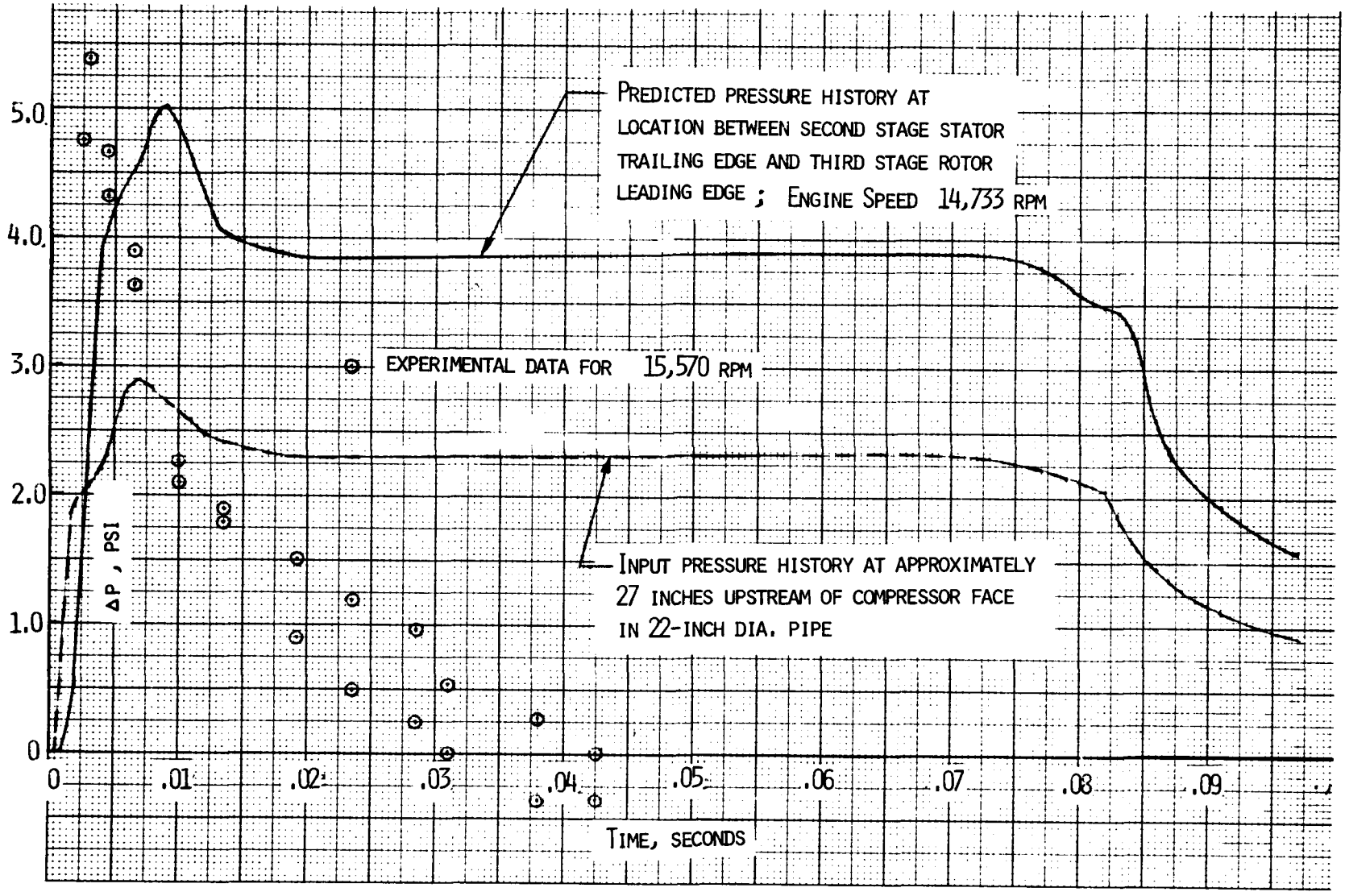

Figure 21 PRESSURE RESPONSE WITHIN J-85 COMPRESSOR FOR Δp = 2.3 psi

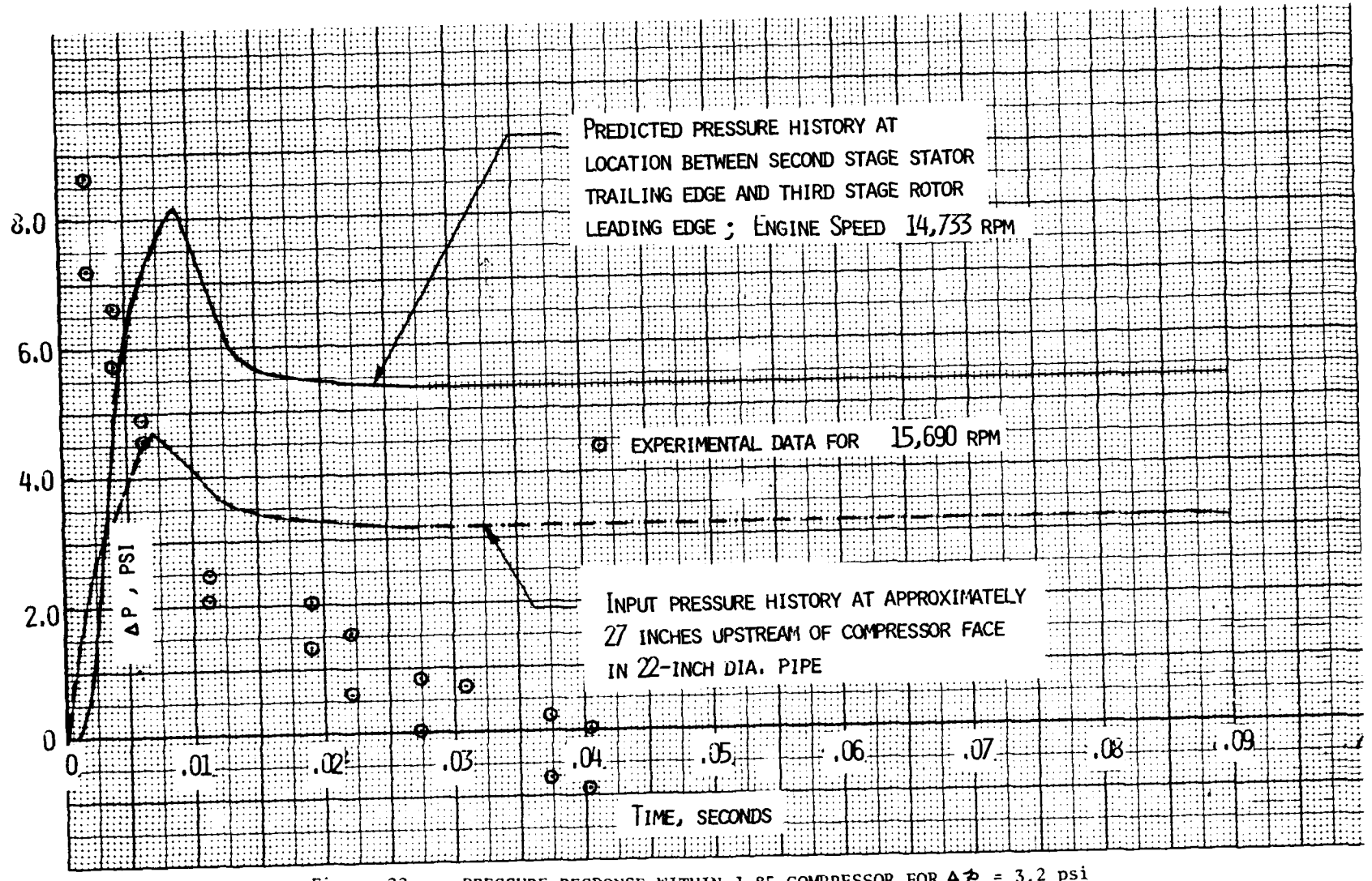

Figure 22 PRESSURE RESPONSE WITHIN J-85 COMPRESSOR FOR $\Delta \bar{p}$ = 3.2 psi

DISTRIBUTION LIST

DEPARTMENT OF DEFENSE

Assistant to the Secretary of Defense
Atomic Energy
ATTN: Executive Assistant

Defense Inelligence Agency
ATTN: DB-4C, V. Fratzke

Defense Nuclear Agency
ATTN: SPAS
ATTN: STSP
4 cy ATTN: TITL

Defense Technical Information Center
12 cy ATTN: DD

Field Command
Defense Nuclear Agency
ATTN: FCPR
ATTN: FCT, W. Tyler

Field Command
Defense Nuclear Agency
ATTN: FCPRL

Undersecretary of Def for Rsch & Engrg
ATTN: Strategic & Space Systems (OS)

DEPARTMENT OF THE ARMY

Harry Diamond Laboratories
Department of the Army
ATTN: DELHD-N-P, J. Gwaltney

U.S. Army Ballistic Research Labs
ATTN: DRDAR-BLT, W. Taylor
ATTN: DRDAR-BLT, J. Keefer

U.S. Army Materiel Dev & Readiness Cmd
ATTN: DRCDE-D, L. Flynn

U.S. Army Nuclear & Chemical Agency
ATTN: Library

DEPARTMENT OF THE NAVY

Naval Material Command
ATTN: MAT 08T-22

Naval Research Laboratory
ATTN: Code 2627

Naval Surface Weapons Center
ATTN: Code F31, K. Caudle

Naval Weapons Evaluation Facility
ATTN: L. Oliver

Office of Naval Research
ATTN: Code 465

Strategic Systems Project Office
Department of the Navy
ATTN: NSP-272

DEPARTMENT OF THE AIR FORCE

Aeronautical Systems Division
Air Force Systems Command
ATTN: ASD/ENFT, R. Bachman
4 cy ATTN: ASD/ENFTV, D. Ward

Air Force Aero-Propulsion Laboratory
ATTN: TBC, M. Stibich

Air Force Material Laboratory
ATTN: MBE, G. Schmitt

Air Force Weapons Laboratory
Air Force Systems Command
ATTN: NTV, G. Campbell
ATTN: NTV, A. Sharp
ATTN: NTV, D. Payton
ATTN: SUL

Assistant Chief of Staff
Studies & Analyses
Department of the Air Force
ATTN: AF/SASC, B. Adams
ATTN: AF/SASB, R. Mathis

Deputy Chief of Staff
Research, Development, & Acq
Department of the Air Force
ATTN: AFRDQI, N. Alexandrow

Foreign Technology Division
Air Force Systems Command
ATTN: SDBF, S. Spring

Strategic Air Command
Department of the Air Force
2 cy ATTN: XPFS, F. Tedesco

Assistant Secretary of the Air Force
Deputy for Strategic & Space Systems
ATTN: SAF/ALR, H. Cooper

Air Force Systems Command
ATTN: AFSC/DLWM, B. Almassy
ATTN: AFSC/DLWM, D. Waltman
ATTN: AFSC/DLF, J. Morgan

DEPARTMENT OF ENERGY CONTRACTORS

Sandia National Laboratories
ATTN: A. Lieber

DEPARTMENT OF DEFENSE CONTRACTORS

Boeing Co
ATTN: M/S 85/20, E. York

Boeing Wichita Co
ATTN: R. Syring

Calspan Corp
ATTN: M. Dunn

DEPARTMENT OF DEFENSE CONTRACTORS (Continued)

University of Dayton
Industrial Security Super KL-505
ATTN: B. Wilt

Effects Technology, Inc
ATTN: R. Globus
ATTN: R. Parisse
ATTN: E. Bick

General Electric Company—TEMPO
ATTN: DASIAC

General Electric Company—TEMPO
ATTN: J. Moulton

General Research Corp
ATTN: T. Stathacopoulos
ATTN: J. Cunningham

Kaman Sciences Corp
ATTN: D. Sachs

DEPARTMENT OF DEFENSE CONTRACTORS (Continued)

Kaman AviDyne
ATTN: N. Hobbs
ATTN: E. Criscione
ATTN: R. Ruetenik
ATTN: B. Lee

Los Alamos Technical Associates, Inc
ATTN: B. Myers
ATTN: C. Sparling
ATTN: P. Hughes

Prototype Development Associates, Inc
ATTN: C. Thacker
ATTN: J. McDonald

R & D Associates
ATTN: F. Field
ATTN: C. MacDonald
ATTN: A. Kuhl
ATTN: P. Rausch
ATTN: P. Haas